iScience

Article

CD28 signaling domain boosts persistence and *in vivo* anti-tumor activity of stem cell-derived CD19-CAR-NK cells

Graphical abstract

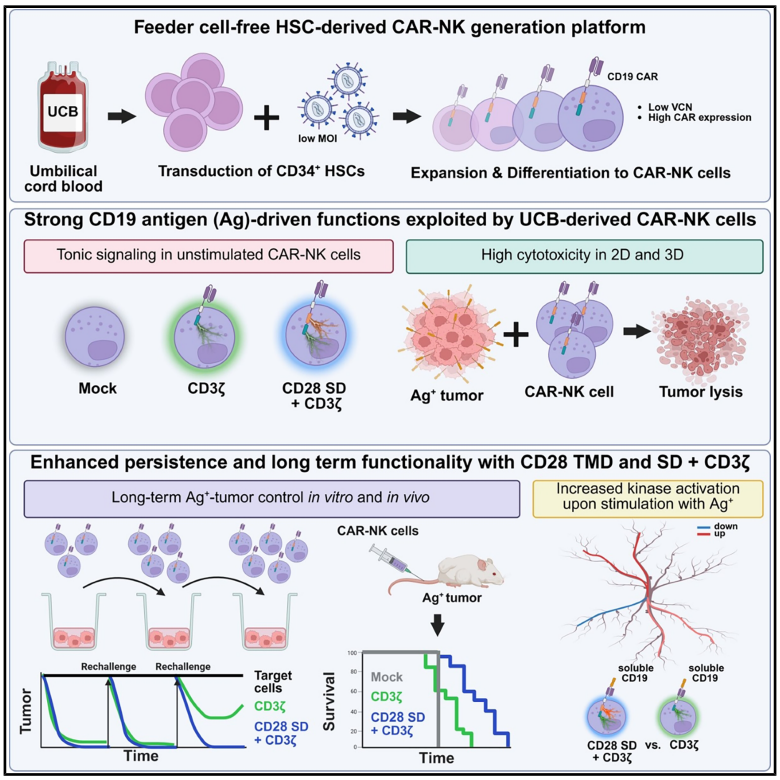

Highlights

- High and stable CAR expression in feeder free UCB-HSC-derived NK cells
- CAR-specific tonic signaling preconditions NK cells for antigen-specific responses
- CD28 signaling domain (SD) enhances CAR-NK differentiation and ADCC potential
- CD3ζ and CD28 SDs in CAR-NK show enhanced persistence and *in vivo* tumor control

Authors

Nina Kok, Didem Ozkazanc, Amanda A. van Vliet, ..., Monica Raimo, Jan Spanholtz, Adil Doganay Duru

Correspondence

adil@glycostem.com

In brief

Natural sciences; Biological sciences; Immunology; Systems biology; Cancer systems biology

Kok et al., 2025, iScience *28*, 112548
June 20, 2025
https://doi.org/10.1016/j.isci.2025.112548

CellPress

iScience

CellPress
OPEN ACCESS

Article

CD28 signaling domain boosts persistence and *in vivo* anti-tumor activity of stem cell-derived CD19-CAR-NK cells

Nina Kok,[1,4] Didem Ozkazanc,[1,4] Amanda A. van Vliet,[1] Danielle Steenmans,[1] Simar Pal Singh,[2] Tolga Sutlu,[3] Anna-Maria Georgoudaki,[1] Monica Raimo,[1] Jan Spanholtz,[1] and Adil Doganay Duru[1,5,*]

[1]Glycostem Therapeutics B.V., Oss, the Netherlands
[2]Pamgene International B.V., 's-Hertogenbosch, the Netherlands
[3]Acibadem University, Istanbul, Turkiye
[4]These authors contributed equally
[5]Lead contact
*Correspondence: adil@glycostem.com
https://doi.org/10.1016/j.isci.2025.112548

SUMMARY

Allogeneic natural killer (NK) cell-based therapies with an outstanding safety profile, are a compelling alternative to autologous T cell-based approaches for cancer immunotherapy, offering innate tumor-killing ability that can be further augmented via introduction of tumor antigen-specific chimeric antigen receptors (CARs). In this study, we genetically engineered primary human hematopoietic stem cells using an optimized lentiviral backbone carrying CD19 CAR cassettes with varied hinge, transmembrane, and signaling domains to evaluate their role in CAR-NK development and function. Our platform integrates early genetic modification with our unique expansion/differentiation system, enabling high CAR expression with low vector copy numbers. Notably, CARs incorporating CD28 transmembrane and signaling domains with CD3ζ, promoted enhanced tonic signaling, accelerated NK differentiation, enhanced antigen-specific kinome activation, and improved cytotoxicity and persistence both *in vitro* and *in vivo*. These findings offer a robust strategy for development of stem cell-based CAR-NK immunotherapies, combining potent innate, and antigen-specific antitumor responses.

INTRODUCTION

Initially developed for retargeting T cells, the introduction of antigen specificity by chimeric antigen receptor (CAR) technology spotlights natural killer (NK) cells as a highly advantageous tool for adoptive cell therapy due to their favorable safety profile. Despite promising clinical outcomes of CAR-T cells targeting CD19 and B cell maturation antigen (BCMA), CAR-T therapies are associated with severe side effects, such as cytokine release syndrome (CRS), prolonged low blood counts, and neurologic toxicities, as well as the risk of forming product-related secondary malignancies in the autologous setting.[1] In contrast, it has been demonstrated in multiple academic- and industry-led clinical studies that NK cell infusions generally have no risk of causing graft-versus-host disease (GvHD) or CRS,[2] even if used in an unmatched allogeneic setting.[3] The safety profile, coupled with their potent antitumor activity mediated by a multimodal arsenal of tumoricidal mechanisms, position NK cells at the forefront of next-generation CAR/TCR-based cancer immunotherapy development.

Genetic modification of NK cells has been historically challenging, using retroviral and lentiviral vectors, due to their inherent antiviral defense mechanisms.[4] Several studies have exploited strategies, such as targeting intracellular antiviral defense mechanisms[5] or prior conditioning with cytokine cocktails or feeder cells.[6] Some other strategies encompass different envelope proteins to pseudo-type the viral particles (e.g., vesicular stomatitis virus G protein [VSV-G] or Baboon envelope [BaEV]) to modify terminally differentiated NK cells for the development of engineered NK cell based therapeutic products.[6] Additionally, in order to deliver large numbers of genetically engineered NK cells in a GMP compliant setting, combination of genetic engineering methods with efficient NK cell expansion protocols should be examined closely, as it was systematically demonstrated that the choice of gene delivery enhancers and NK cell pre-stimulation might abrogate the subsequent expansion of transduced cells.[7]

Implementing CAR technology to NK cells requires NK-oriented CAR-cassette development to select the optimal promoter, hinge region, transmembrane domain (TMD), and signaling domains (SD) to potentiate efficient tumor targeting, while preserving the innate cytotoxicity mechanism of NK cells. However, the use of different starting materials and the differences in the various platforms for CAR-NK cell generation, do not allow a direct comparison of the various CAR designs used in order to identify the optimal construct elements for efficient

CAR-NK cell generation.[2,8,9] While initial CAR-NK studies inherited the use of CD3ζ TMD and activation domains that were based on first generation CAR-T designs,[1] advanced iterations have explored various hinge domains (e.g., CD8α, IgG, CD28) and SDs, such as CD28, 4-1BB, CD3ζ, OX40, ICOS, CD27 as well as NK-specific SDs, such as DAP10, DAP12, 2B4, and FcRγ. NK cell receptor-derived TMD and SD originating from 2B4,[10] NKG2D,[11] DAP10, and DAP12[12–14] have shown promising *in vitro* and *in vivo* efficacy. Unfortunately, there are only a handful of studies comprehensively comparing these elements in a systematic way, all leveraging the NK-92 cell line for testing of CAR constructs,[15] and then transferring them to NK cells from other sources like iPSC-[16] and cord blood-derived NK cells.[17] Overall, most CAR-NK studies use CD8α hinge and CD28 TMD domain in combination with SD from CD28 and/or 4-1BB, followed by the CD3ζ activation domain.

The generation of CAR-NK cells from hematopoietic stem cells (HSCs), and specifically from umbilical cord blood (UCB)-derived CD34$^+$ cells, remains relatively unexplored. Limited knowledge exists regarding the optimal conditions and genetic constructs necessary to produce functional CAR-NK cells from these progenitor cells.[18–20] One pioneering study proposing to modify HSPCs with anti-CD19 CAR presented a perspective to sustain long-term transgene persistence and generated antigen-specific effector cells of multiple lineages (myeloid or NK cells).[19] However, this study investigated *in vitro* and *in vivo* differentiation of modified HSCs into different lineages and was not focused on investigating and optimizing the generation of clinically relevant amounts of CAR-NK cells. Thus, current knowledge on generating efficient and functional CAR-NK cells using HSCs as start material is limited.

In this study, we aimed to address this gap of knowledge systematically by focusing on the design and optimization of an in-house developed VSV-G pseudotyped lentiviral vector to identify a functionally optimal and universal CAR cassette for generation of CAR-NK cells from primary UCB-derived CD34$^+$ HSCs. Utilizing Glycostem's established feeder cell-free process for the expansion and differentiation of NK cells,[21,22] we integrated an LV transduction step targeting HSCs to achieve stable and sustained transgene expression throughout stem cell expansion and differentiation to NK cells, thus significantly reducing the quantity of LV particles used and improving safety by decreasing the vector copy number (VCN) per cell. Furthermore, different promoters, namely EF1a, MNDU3, SV40, CMV, and PGK, and different CAR cassette components, such as CD8α and IgG hinges, CD3ζ, CD28, and 4-1BB TMDs, CD28, and 4-1BB SD and CD3ζ SD, have been evaluated. Briefly, we demonstrated that CD8α hinge followed by CD28 TMD and SD coupled with CD3ζ SD, driven by the MNDU3 promoter, provide optimal stable CD19 CAR expression, antigen-specific and innate cytotoxicity, as well as *in vitro* and *in vivo* persistence against the NALM-6 B-ALL model.

To our knowledge, this is the first study demonstrating efficient, stable and highly functional CAR expression using CD34$^+$ HSC as start material for feeder cell-free CAR-NK cell generation which can facilitate further explorations of more NK-oriented CAR designs with additional improvements such as cytokine engineering and introduction of elements contributing to migration and homing or resistance to tumor microenvironment (TME)-driven immunosuppression.

RESULTS

GS lentiviral backbone drives the most stable and sustained transgene expression under MNDU3 promoter after *ex vivo* CD34$^+$ HSC transduction and during differentiation to NK cells

First, we designed a lentiviral transfer plasmid backbone (GS backbone) complying with clinical safety and regulatory guidelines, i.e., containing only the minimal necessary elements for transgene expression in a third-generation self-inactivating (SIN) vector design, and the kanamycin bacterial resistance gene (Figure 1A). We constructed five versions of the GS backbone, each with a different promoter upstream of enhanced green fluorescent protein (eGFP), to identify the optimal promoter driving stable transgene expression during NK cell differentiation. CD34$^+$ HSCs were transduced with these five lentiviral constructs at MOI 20 and further expanded and differentiated into genetically modified (GM) NK cells (Figure 1B). One-week post-transduction, we observed eGFP expression in more than 80% of the CD45$^+$ cells for all promoters except for SV40, with the highest signal intensity (measured as ΔMFI, see STAR Methods for calculation) observed for MNDU3 (Figures 1C and 1D). There was a significant reduction in eGFP expression and/or signal intensity for all promoters after week 1 post-transduction, but overall expression remained stable between week 2 and week 5, except for a temporary loss at week 3 for MNDU3, at week 4 for PGK, and week 5 for CMV (Figures 1F and 1G). CMV showed loss of expression after week 3, while EF1α and SV40 showed a similar trend of partial recovery of expression in the final week, although SV40 showed the lowest expression overall (Figures 1C and 1D). Flow cytometry-based analysis of eGFP expression driven by the five promoters at 3-week post-transduction showed that MNDU3, EF1α and PGK exhibited not only pronounced transgene expression but also the most distinct separation between transduced and non-transduced cell populations, with the highest separation observed for eGFP expression under the MNDU3 promoter (Figures 1C–1H). Transduced cells show comparable levels of CD56 expression ($\geq$82.0%) at the end of 5 weeks (Figure 1E). Together, these data show how genetic modification of early progenitor cells with the GS lentiviral backbone leads to sustained transgene expression through the NK cell differentiation process, and that particular attention must be given in choosing the appropriate promoter. For the rest of the study, we selected the GS backbone with the MNDU3 promoter as it was identified as the most optimal promoter for CAR expression based on the aforementioned assessments.

Anti-CD19 CAR constructs under MNDU3 promoter drive stable CAR expression and exerts antigen-specific functionality in the NK-92 cell line

To evaluate the efficiency of the MNDU3-GS backbone in generating antigen-specific NK cells, we designed three different codon-optimized anti-CD19 CAR cassettes, all

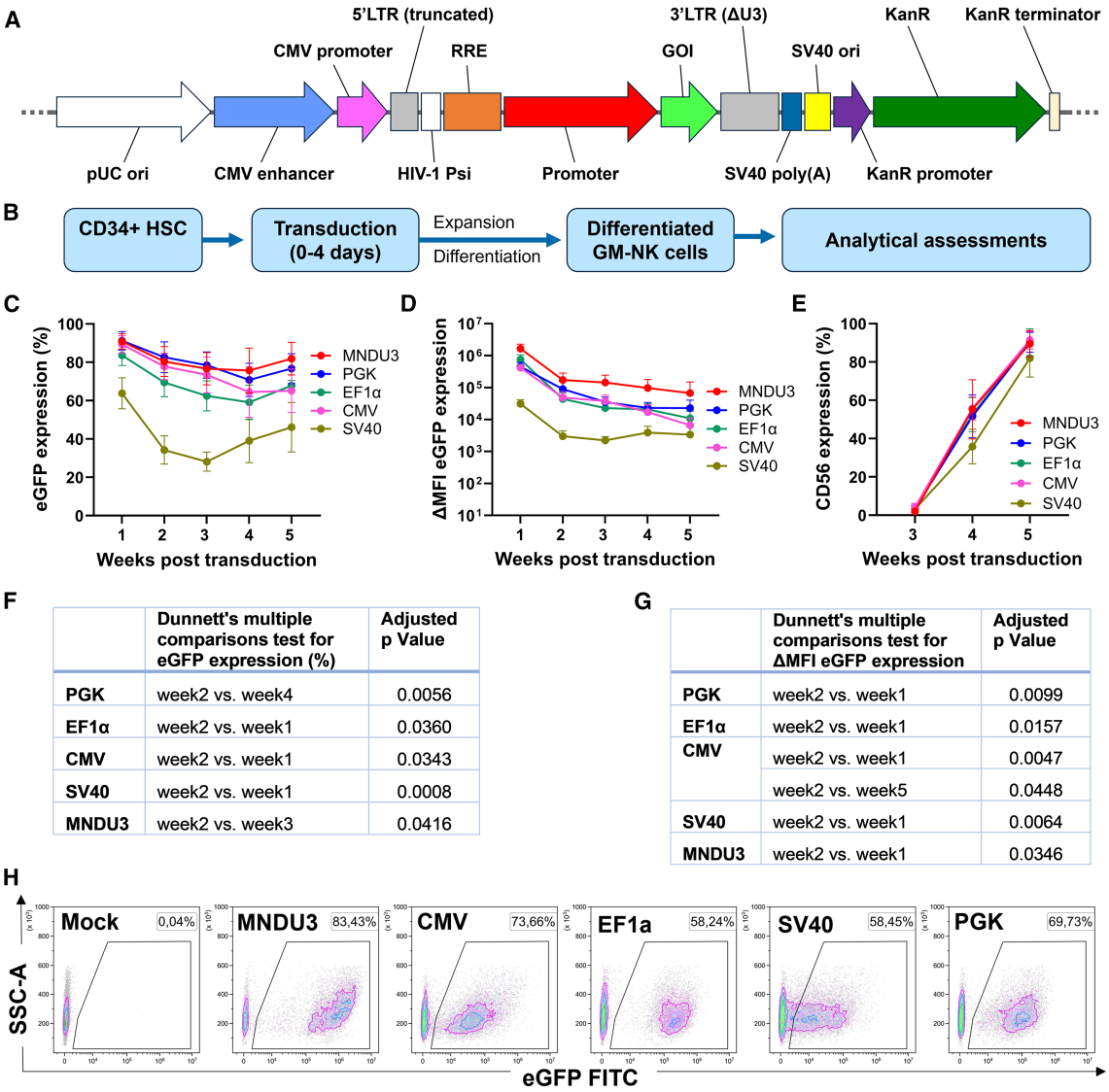

F

	Dunnett's multiple comparisons test for eGFP expression (%)	Adjusted p Value
PGK	week2 vs. week4	0.0056
EF1α	week2 vs. week1	0.0360
CMV	week2 vs. week1	0.0343
SV40	week2 vs. week1	0.0008
MNDU3	week2 vs. week3	0.0416

G

	Dunnett's multiple comparisons test for ΔMFI eGFP expression	Adjusted p Value
PGK	week2 vs. week1	0.0099
EF1α	week2 vs. week1	0.0157
CMV	week2 vs. week1	0.0047
	week2 vs. week5	0.0448
SV40	week2 vs. week1	0.0064
MNDU3	week2 vs. week1	0.0346

Figure 1. The GS lentiviral plasmid supports sustained transgene expression during CD34⁺ HSC differentiation to NK cells under multiple promoters

(A) Linear map of the GS lentiviral plasmid backbone. Five different promoters (CMV, MNDU3, PGK, EF1a, and SV40) driving gene expression were compared. Ori: origin of replication; CMV: cytomegalovirus; LTR: long terminal repeat; HIV-1: human immunodeficiency virus type-1; Psi: viral packaging signal sequence; RRE: Rev response element; GOI: gene of interest; SV40: simian vacuolating virus 40; poly(A): polyadenylation signal; KanR: kanamycin resistance.

(B) Workflow of the generation of genetically modified (GM) NK cells from CD34⁺ HSCs.

(C and D) eGFP expression, driven by one of the five promoters, during weeks 1–5 of NK cell differentiation after HSC transduction at MOI20, expressed as (C) percentage of eGFP expressing CD45⁺ cells and as (D) intensity of eGFP signal (ΔMFI) (n = 3 donors).

(E) NK differentiation measured as CD56 expression % of transduced cells, between week 3–5 (n = 3 donors).

(F and G) The tables represent p values of the statistically significant differences between week 2 and every other week (1–5) post-transduction for (F) percentage of eGFP and (G) intensity of eGFP signal (ΔMFI) calculated using Two-way ANOVA with Dunnett's multiple comparisons test.

(H) Representative flow cytometry dot plots of eGFP expression (FITC channel) under different promoters at week 3 post-transduction of CD34⁺ cells. Mock cells went through the same transduction process (minus lentiviral supernatant) and culture scheme as transduced cells and served as a negative control. Data are shown as mean ± SD.

containing a CD8α hinge region. CAR1 is containing a CD3ζ TMD and SD, CAR2 has CD28 TMD and SD linked to CD3ζ and CAR3 has 4-1BB TMD and SD connected to CD3ζ SD (Figure 2A) and all constructs contained an FLAG tag for CAR detection. Transduction efficiency and functionality of these CAR constructs were first evaluated using the NK-92 cell line (Figures 2B–2F). While CAR1 and CAR2 constructs showed high CAR expression (with over 50% transduction efficiency over 3 weeks), CAR3 cassette containing 4-1BB TMD and SD only reached up to 20% CAR expression, and NK-92 cells

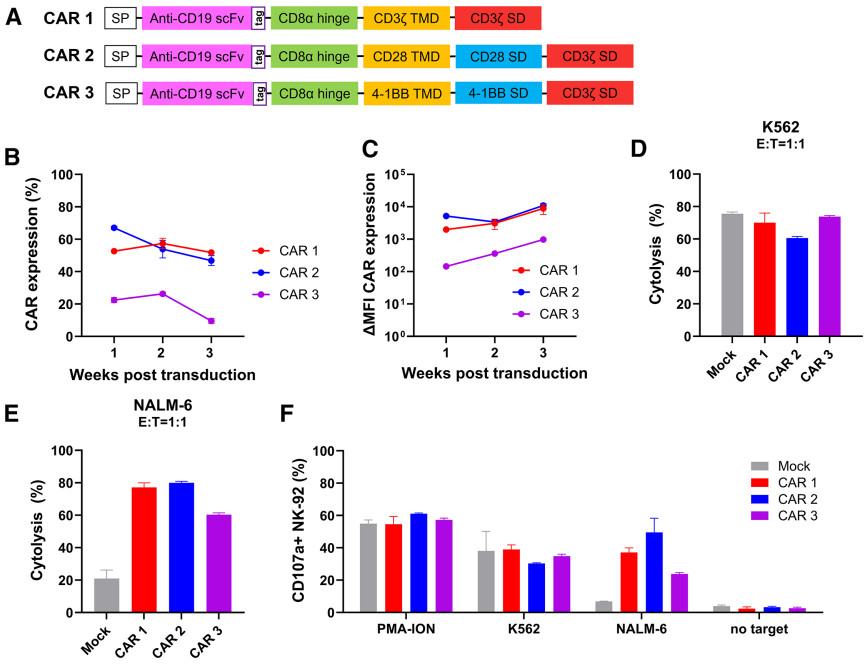

Figure 2. MNDU3-GS anti-CD19 CAR constructs are stably expressed and show antigen-dependent functionality on a model cell line, NK-92

(A) Schematic representation of cassette design for CARs 1, 2, and 3. Elements: SP, signal peptide; anti-CD19 scFv, single-chain variable fragment; tag, FLAG tag; CD8α hinge; CD3ζ, CD28, and 4-1BB TMD, transmembrane domain; CD28 and 4-1BB SD, signaling domains; and CD3ζ SD.

(B) Percentage of CAR-expressing cells and (C) average expression level (ΔMFI) for the three CAR constructs on transduced CD56$^+$ NK-92 cells at MOI20 during a period of 3 weeks post transduction (one independent experiment in technical replicates) (CAR expression for Mock below 3%, not shown).

(D and E) Cytotoxicity of CD19 CAR engineered NK-92 cells against (D) CD19$^-$ K562 cells or (E) CD19$^+$ NALM-6 cells determined at 5 h with a flow-based cytotoxicity assay at an E:T ratio of 1:1 (two independent experiments in technical triplicates).

(F) 5 h degranulation assay at an E:T ratio of 1:1 (two independent experiments in technical triplicates), for which the control PMA-ION is depicting the maximum degranulation status and the control no target is depicting the lowest degranulation status. Data are shown as mean ± SD.

failed to stably express CAR3 resulting in a very low CAR expression 3 weeks post transduction (Figure 2B) and a similar trend in between different cassettes has been observed for CAR expression levels among CAR$^+$ populations, reported as ΔMFI, over 3 weeks (Figure 2C). Additionally, the cytotoxicity of Mock control and CAR transduced cells was determined in a 5 h flow cytometry-based cytotoxicity assay by assessing their response to NK-sensitive CD19$^-$ K562, and NK-resistant CD19$^+$ NALM-6 tumor cells with confirmed CD19 surface expression (Figure S1B). All different CAR-NK cells maintained their natural cytotoxicity in recognizing and lysing K562 cells, with CAR1 showing 70.1% ± 5.9% cytotoxicity, CAR2 60.6% ± 1.0%, and CAR3 73.8% ± 0.6%, demonstrating a similar cytolytic capacity as Mock cells 75.6% ± 1.1% except a slight decrease in killing of K562 cells by CAR2 in 5 h (Figure 2D). Against the CD19$^+$ NALM-6 cell line, all constructs selectively triggered antigen-specific effector functions at E:T ratio of 1:1, with CAR1 exerting 77.1% ± 2.8% cytotoxicity, CAR2 80.0% ± 0.9%, and CAR3 60.4% ± 1.1%, whereas Mock cells showed only 21.0% ± 3.0% cytotoxicity (Figure 2E). Furthermore, significantly higher NK cell degranulation was also observed in a 5 h assay at E:T (1:1) against NALM-6 cells for all CARs, with the highest degranulation for CAR2 (49.5%), followed by CAR1 (37.1%), and CAR3 (23.8%). Overall, CAR3 with 4-1BB TMD and SD induced lower CD19-specific effector functions against NALM-6 cells, possibly due to low CAR$^+$ cell numbers. Additionally, degranulation of CAR2 was slightly lower at E:T (1:1) against K562 (Figure 2F). Overall, expression and functional profile of MNDU3-GS anti-CD19 CAR constructs in NK-92 cells demonstrated the capacity and the potential of these novel constructs for further exploration on CD34$^+$-derived NK cells.

Potent antigen-specific cytotoxicity of CD19 CAR-NK cells facilitated by stable CAR expression during NK cell differentiation while maintaining antigen-independent functionality

Having demonstrated efficient transduction of early-stage cells (Figure 1), and stable and functional expression of MNDU3-GS anti-CD19 CARs in NK-92 cells (Figure 2), we next transduced primary CD34$^+$ cells isolated from UCB with CAR1, CAR2, or CAR3 at MOI 20, followed by expansion and NK differentiation. CAR expression of all 3 CAR constructs was detected during the 5 weeks post transduction, while Mock cells were CAR (FLAG) negative (Figure 3A). The average transduction efficiency of CD34$^+$-derived cells was 67.2% for CAR1, 75.4% CAR2, and 36.9% for CAR3 1-week post-transduction, which remained relatively stable for 5 weeks for CAR1 and CAR2 but decreased to < 10% in weeks 4–5 for CAR3 (Figure 3A). The ΔMFI for CAR1 and CAR2 were higher than for CAR3, for which also the ΔMFI was slightly dropping during differentiation (Figure 3B).

Differences in NK cell differentiation was also observed, especially around week 3, showing enhanced maturation for CAR1 and CAR2 transduced cells, compared to Mock and CAR3, but all cultures reached ≥ 98% CD56 expression by week 5 (Figures 3C and 3D). This enhanced speed of differentiation was particularly seen for CAR2, using a larger donor set (n = 9), suggesting a favorable role of the CD28 SD component in influencing *ex vivo* NK differentiation potentially positive due to tonic signaling (Figure S3A). Additionally, significantly higher CD16 expression was detected on CAR2 cells compared to Mock, during weeks 3–5 post transductions (Figure S3B).

For functional analyses, CAR-NK and Mock cells were co-cultured at 1:3 and 1:10 (E:T ratio) either with CD19$^-$ K562 or CD19$^+$ NALM-6 tumor cells for a comparative analysis of natural

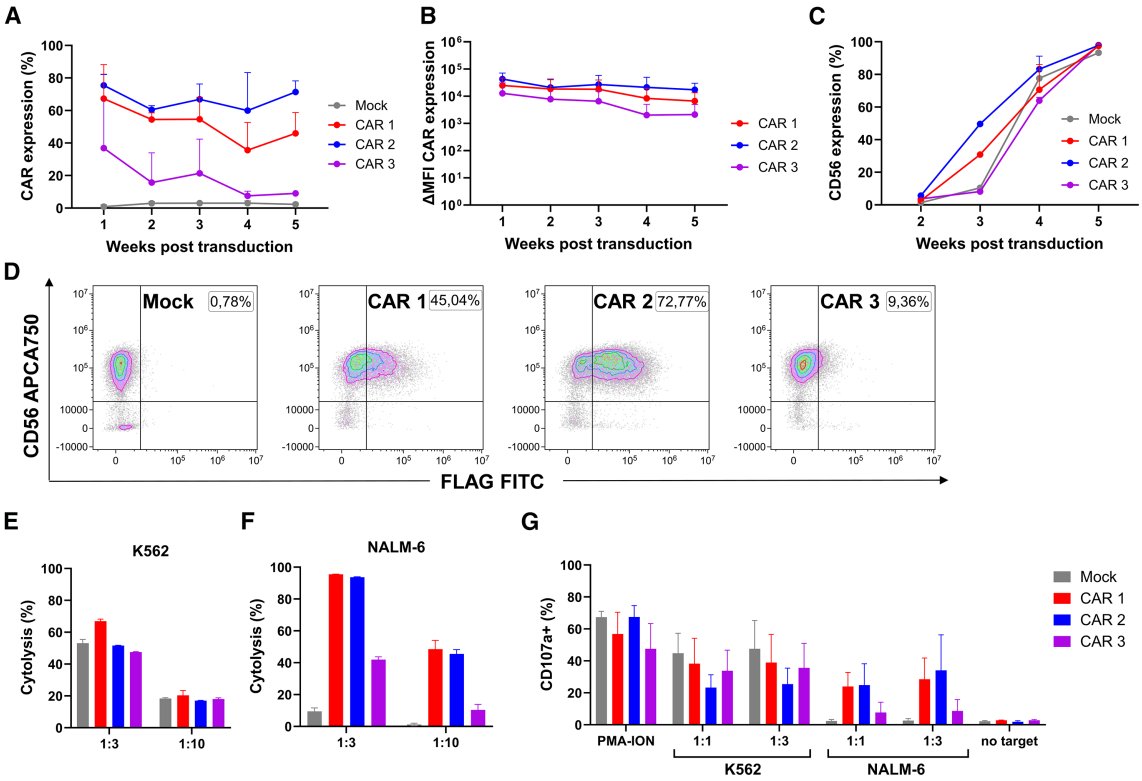

Figure 3. MNDU3-GS anti-CD19 CAR constructs are stably expressed and show antigen-dependent functionality on CD34⁺ HSC-derived NK cells

(A) Percentage of CAR expression (CARs 1, 2, and 3) and (B) average CAR expression level (ΔMFI) on CD34⁺-derived cells through 5 weeks of culture to NK differentiation (n = 2 donors, two independent experiments) (MOI20).

(C) NK differentiation of transduced and Mock cells, starting from week 2 (n = 2 donors, two independent experiments). CD56⁺ cells were gated from ViaKrome808⁻/CD45⁺ cells.

(D) Representative dot plots of CAR expression at week 5 post-transduction. CAR positive cells, detected via FLAG antibody, were pre-gated from ViaKrome808⁻/CD45⁺ cell population and plotted against CD56.

(E and F) CAR-NK and Mock cell cytotoxicity analysis assessed after 24 h via flow cytometry against (E) CD19⁻ K562 and (F) CD19⁺ NALM-6 with E:T ratios of 1:3 and 1:10 (n = 2 donors, two independent experiments in technical triplicates).

(G) 5 h flow cytometry degranulation assay against K562 and NALM-6 at E:T ratios of 1:1 and 1:3 (statistical analysis was performed using two-way ANOVA with Tukey test to compare different CARs among each condition and no trend was determined) (n = 2 donors, two independent experiments in technical triplicates). PMA and ionomycin (PMA-ION) were used to stimulate degranulation. Data are shown as mean ± SD.

and antigen-specific cytotoxicity, respectively (Figures 3E and 3F). CAR1 showed increased cytotoxicity against K562 using a 1:3 E:T ratio, which was not detected in a more challenging E:T ratio of 1:10 (Figure 3E). All CAR constructs showed antigen-dependent lysis of NALM-6 cells compared to Mock cells (Figure 3F), however, for CAR3 cytotoxicity, the levels remained notably lower than that of CAR1 and CAR2, possibly resulting from its lower CAR expression. This finding was confirmed by CD19 antigen-dependent degranulation responses of CAR-NK cells against NALM-6 tumor cells at 1:1 and 1:3 E:T ratios (Figure 3G). Collectively, these experimental data suggest that the design of CAR3, carrying the 4-1BB TMD and SD domains (Figure 2A), negatively impacts both CAR stability and functionality of CD34⁺ derived CAR-NK cells. On the other hand, for CAR1 and CAR2 either containing a CD3ζ TMD and SD or a CD28 TMD/SD and CD3ζ SD, respectively, (Figure 2A), stable and functional CAR expression is observed. As TMD and SD are important components of the CAR design that ensure the stability needed for robust CAR expression, as well as provide a critical level of activation signals to elicit potent and persistent antitumor function of CAR-NK effector cells, we next decided to evaluate the role of CD28 TMD and/or SD components in combination with CD3ζ SD. We also decided not to pursue 4-1BB TMD and SD domains based on CAR stability and -functionality data with both NK-92 cells and CD34⁺ HSC-derived NK cells (Figures 2 and 3).

Additionally, while MOI of 20 already led to high and stable transduction of CD34⁺ cells and reliable and functional CAR expression on differentiated NK cells (Figure 3), we aimed to identify lower MOIs (range 0.5–5) still leading to stable CAR expression but potentially contributing to an increased safety profile by having less integrations measured as VCN using CAR2 (Figure S2A). MOIs between 2 and 5 gave rise to more than 50% CAR positive cells, whereas a MOI of 1 or below still resulted in about 30% CAR-NK cells. Moreover, a linear correlation between CAR expression and log MOI and VCN for CAR2

depicted in Figure S2B showed VCNs below 3 for the MOI range of 0.5–5. Therefore, we proceeded to perform all future experiments with an MOI of 5.

Optimized CD19 CAR constructs improve CAR expression levels, stability, and efficacy with preserved functionality post cryopreservation

To further evaluate the role of different TMDs (CD3ζ or CD28) and SDs (CD3ζ only or CD3ζ and CD28), we compared CAR1 and CAR2 with a new CAR4 cassette design, which contained only CD28 TMD and CD3ζ SD (Figure 4A), side by side for multiple donors in terms of NK cell differentiation, stability of CAR expression levels and cytotoxic potential. Transduction efficiencies for all constructs were between 60% and 80% 1 week after transduction and CAR levels remained considerably stable over the course of 5-week post-transduction until the completion of the NK expansion and differentiation process (Figure 4B). CAR2 and CAR4 constructs containing CD28 TMD demonstrated comparably higher CAR expression level, and specifically for CAR4, containing the CD28 TMD and CD3ζ SD, also showed an increased ΔMFI and a clear separation of CAR^+ from CAR^- populations (Figures 4B, 4C, and 4E). Additionally, Mock and CAR-transduced cells show comparable levels of CD56 expression (≥97.8%) at the end of 5 weeks but with faster differentiation rate of CAR2 transduced cells (Figure 4D).

Next, we evaluated functional characteristics of different CAR-NK cells and Mock cells against either NALM-6 or K562 cells (Figures 4F and 4G). The CD19 antigen-directed *in vitro* cytotoxicity was measured as 12.2% ± 5.9% for Mock cells, at 59.0% ± 0.8% for CAR1 and at 59.0% ± 0.8% CAR2, whereas CAR4 exerted significantly higher cytotoxicity at 77.3% ± 4.7% (Figure 4F). Quantification of cytotoxic activity against K562 revealed, that innate cytotoxicity was preserved for all CAR-NK constructs (95.6% ± 0.2% for Mock, 94.6% ± 1.0% for CAR1, 83.8% ± 8.8% for CAR2, 89.5% ± 5.7% for CAR4) (Figure 4G). Typically, there are no major changes regarding the signature of CAR-NK cells vs. Mock in terms of expression of important activating receptors, however, changes in expression levels of CD16, NKp44, and TRAIL for the CAR2 construct, has been observed (Figures S4A–S4D). Additionally, evaluation of intracellular levels of IFN-γ, TNF, and release of granzyme B and perforin, which are typical NK cell effector molecules, provided proof that transducing $CD34^+$ NK cells with CAR constructs did not hamper the granular load and the innate functional response capacity when challenged with $CD19^-$ K562 cells (Figure S5A). On the other hand, all CAR constructs demonstrated targeted NALM-6 cells efficiently but CAR2 facilitated (1) increased levels of CD107a (20.9%) and TNF (17.2%) as well as (2) higher perforin release (24.0%) after 5 h of co-culture with NALM-6 cells (Figure S5B).

Having observed the positive impact of the CD28 TMD on stability, expression, and effector function, we further explored CAR2 and CAR4 stability after cryopreservation which potentially facilitates development of off-the-shelf allogeneic CAR NK therapies. Flow cytometry-based count of live NK cells at 3 days and 7 days post-thaw showed that CD19 CAR-NK cells are capable of more efficient recovery and can further expand compared to Mock cells (Figure 4H). Moreover, CAR expression remained mostly stable for CAR4 and was restored to initial levels for CAR2 by the end of the 7-day post thaw recovery process (Figure 4I). Functional assessment of cytotoxicity against K562 and NALM-6 cells provided evidence that CD19 CAR-NK cells retained their cytotoxic potential for antigen-specific and non-specific killing after 7 days of post thaw recovery, with cytotoxicity reaching up to 75% at the E:T ratio of 1:1 in a 5-h assay (Figure 4J). Hence, it was confirmed that the CD28 TMD of the CAR construct is important to induce robust and stable CAR expression as well as to preserve substantial levels of antigen-specific cytotoxicity in GM primary $CD34^+$-HSC-derived NK cells both in fresh and recovered state post cryopreservation.

Additionally, to further investigate the effect of a different hinge domain (HD) in CD28 TMD containing CAR2 and CAR4, new constructs were designed to replace CD8α hinge by IgG1 hinge. Comparative analysis of CAR expression over 5 weeks post transduction revealed that CAR expression and stability for CAR2 is not impacted by swapping CD8α hinge to IgG1 hinge. On the other hand, replacing CD8α hinge with IgG1 hinge on CAR4 showed reduced CAR expression, with more than 40% loss in CAR expression 5 weeks post transduction (Figures S6A and S6B). Based on these results, the follow-up experiments continued using CD19 CAR constructs with CD8α hinge.

Signaling through CD3ζ domain is necessary for CAR-mediated tonic signaling and cytotoxicity but does not affect NK cell phenotype and non-CAR-mediated functionality

We have demonstrated that CD28 TMD together with CD3ζ SD (CAR4) constitutes a compact, stable and potent CAR cassette for $CD34^+$ HSC-derived NK cells, especially superior against CD3ζ or 4-1BB TMD containing cassettes. While further comparison of CAR4 with CD28 SD containing CAR2 is yet to be performed, we next investigated the role of CD3ζ SD's immunoreceptor tyrosine-based activation motives (ITAM) domains on (1) antigen-specific CAR-mediated NK cell cytotoxicity, (2) NK cell phenotype, and (3) innate NK cell cytotoxicity as well as (4) tonic and antigen-mediated signaling. For this purpose, we designed a new construct with mutated CD3ζ SD ITAMs that is unable to facilitate tyrosine-mediated signaling (CAR6) and compared it to CAR5, which is a derivative of CAR4 cassette without the FLAG tag (Figure 5A). A G4S linker antibody was used to detect CAR expression and comparison of FLAG and G4S based CAR detection indicated similar expression profiles (Figure S1A).[23]

$CD34^+$ cells were efficiently transduced with both CAR5 and CAR6, and CAR expression was followed over the 5-week period post transduction with 55.5% ± 13.5% for CAR5 and 77.0% ± 8.9% for CAR6 at week 5, respectively (Figure 5B), with a clear separation of CAR^+ and CAR^- NK cell populations (Figure 5E). CAR expression levels also remained sufficiently high (Figure 5C) and neither the removal of FLAG tag, nor the introduction of mutations in CD3ζ SD effect NK cell differentiation (Figure 5D). Functional assessments showed that CAR6 with CD3ζ mutations failed to induce significant antigen-specific

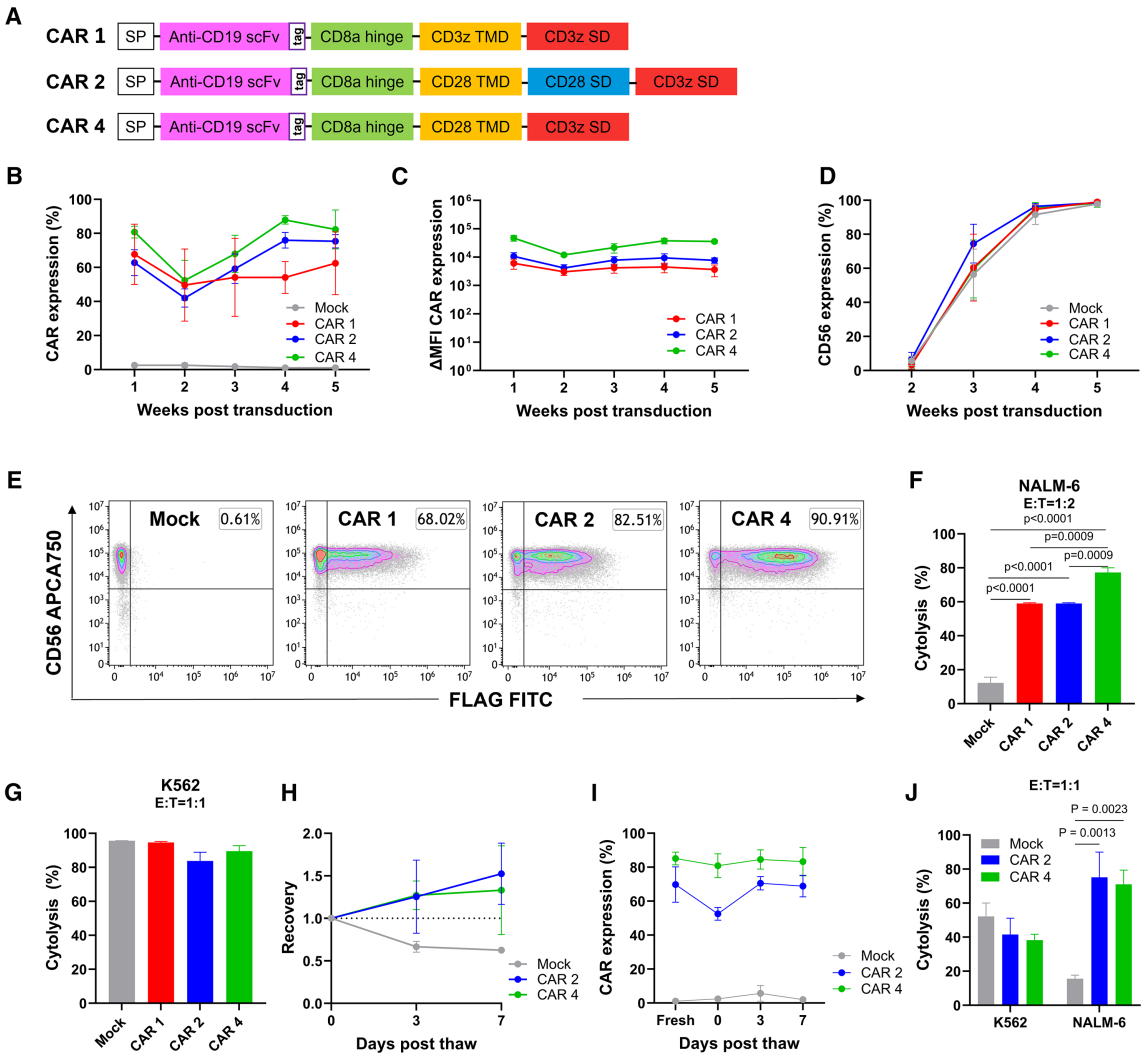

Figure 4. CAR cassette optimization improves expression, stability and efficacy of CAR-NK cells while preserving natural cytotoxicity, also after cryopreservation

(A) Schematic representation of cassette design for CARs 1, 2, and 4.

(B) Percentage of CAR expression and (C) average CAR expression (ΔMFI) over 5 weeks post HSC transduction (MOI5) (n = 3 donors, one independent experiment).

(D) NK differentiation of transduced and Mock cells, starting from week 2 (n = 4 donors, two independent experiments).

(E) Representative dot plots of CAR expression at week 5 post-transduction. CAR positive cells, detected via anti-FLAG antibody were pre-gated from the ViaKrome808$^-$/CD45$^+$ cell population and plotted against CD56.

(F and G) CAR-NK and Mock cytotoxicity analysis assessed after 24 h via flow cytometry against (F) CD19$^+$ NALM-6 with an E:T ratio of 1:2 or (G) CD19$^-$ K562 with an E:T ratio of 1:1. (n = 3 donors, one independent experiment in technical triplicates) (H) Cell recovery of CAR-NK cells compared to Mock cells up to 7 days after thawing, normalized to post-thaw counts (n = 3 donors, three independent experiments).

(I) Percentage of CAR expression up to 7 days post freeze-thaw (n = 3 donors, three independent experiments).

(J) CAR-NK and Mock cytotoxicity analysis on day 7 recovered cells, assessed after 5 h co-culture with CD19$^-$ cell line K562 and CD19$^+$ cell line NALM-6 with an E:T ratio of 1:1 (n = 3 donors, one independent experiment in technical triplicates). Data are shown as mean ± SD. Statistical analysis was performed using (F and G) one-way ANOVA with Tukey's multiple comparisons test and (J) one-way ANOVA with Sidak's multiple comparisons test.

cytotoxicity against CD19$^+$ NALM-6 cells at a low E:T of 1:3 with a similar cytotoxicity profile of Mock cells, indicating the importance of CD3ζ SD ITAM motifs as part of the CAR construct for the antigen-specific activation of CAR NK cells (Figure 5F). Importantly, the decrease in cytotoxicity was limited to CD19$^+$ NALM-6 cells; against CD19$^-$ K562 cells, both CAR5, CAR6 and Mock showed similar high cytotoxicity, implicating that the innate functionality was not affected in CAR5 and CAR6 (Figure 5G).

As an additional challenge, we further focused on CD19 antigen-specific functionality by comparing Mock, CAR5, and CAR6 NK cells against NALM-6 (Figures 5H and 5I) and Daudi

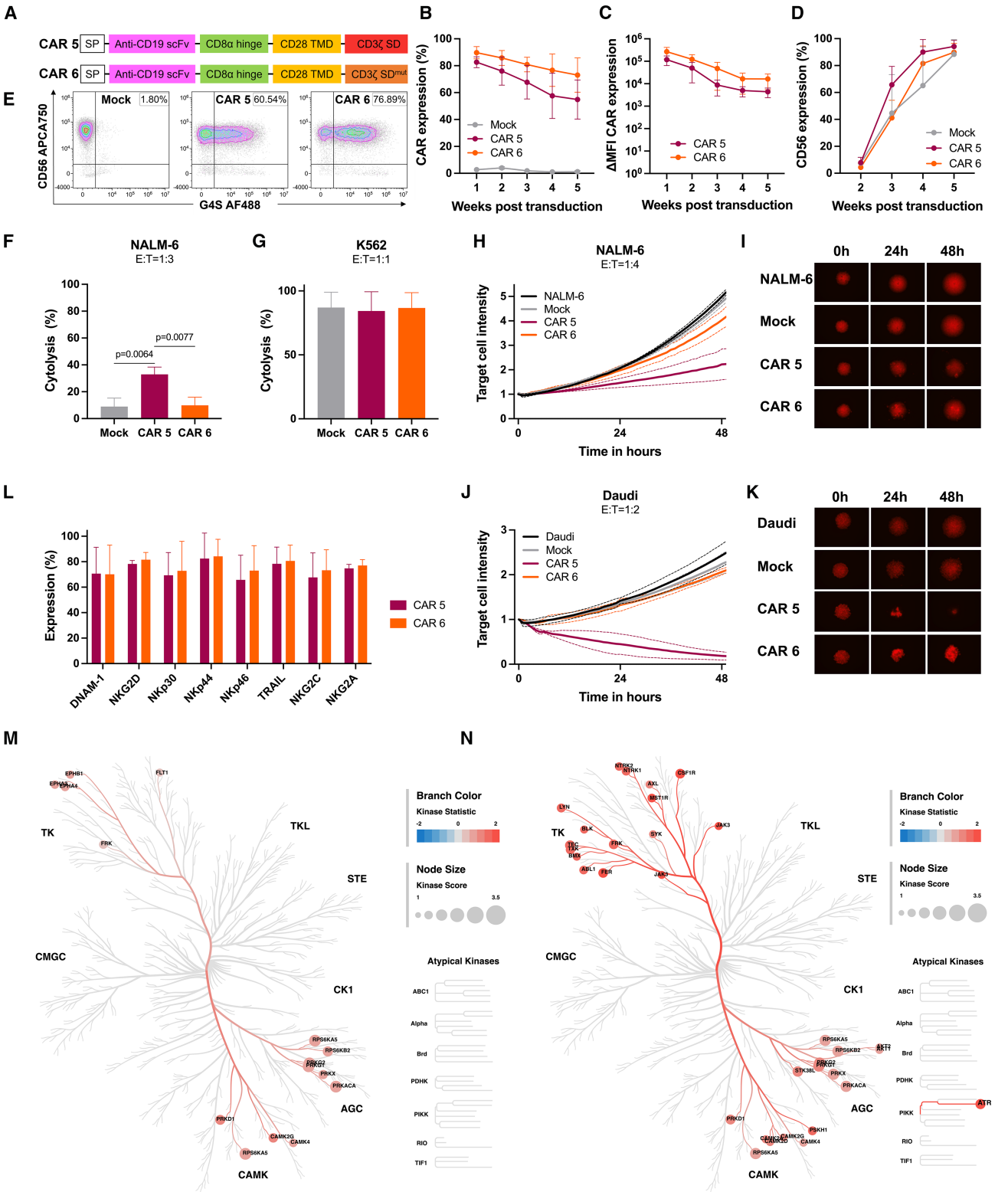

(legend on next page)

(Figures 5J and 5K) tumor cell aggregates in a 3D setting. Robust cytotoxic responses were observed for CAR5 against antigen expressing cell lines NALM-6 and Daudi over 48 h, further confirming the significance of functional CD3ζ signaling for CD19 CAR efficacy in GM primary CD34$^+$-derived NK cells. In contrast, CAR6 performed very similar to Mock control, showing very limited capacity to eliminate both NALM-6 and Daudi aggregates, indicating that abrogation of CD3ζ signaling resulting in dysfunctional CAR-mediated cytotoxicity.

Finally, to understand the impact of CD3ζ SD tonic signaling on the phenotype of CD56$^+$CAR$^+$ cells, we first evaluated the expression of several important NK cell surface markers (Figure 5L). The expression of activating receptors DNAM-1, NKG2D, and NKG2C, natural cytotoxicity receptors NKp30, NKp44, and NKp46, death receptor ligand TRAIL and inhibitory receptor NKG2A was very high for both CAR5 and CAR6 and no significant differences in receptor profile could be detected, suggesting that CD3ζ SD tonic signaling does not impact the assessed NK cell receptor repertoire. Secondly, we performed a detailed kinome analysis of CAR5 and CAR6 containing cells with or without CD19 antigen stimulation using PamChip microarrays, which can track the phosphorylation of 196 protein tyrosine kinase (PTK) and 144 serine/threonine kinase (STK) phospho-sites. A comparative upstream kinase analysis (UKA) of CAR5 and CAR6 cells revealed a CD3ζ SD specific tonic signaling profile including TCR proximal tyrosine kinases (TK) EPHB1, EPHA3, EPHA4, FRK, and FLT1; calcium/calmodulin-dependent kinases (CAMK) PRKD1, RPS6KA5, CAMK2G, and CAMK4 as well as PKA/PKG/PKC-family kinases (AGC) PRKG2, PRKGT, PRKX, PRKACA, RPS6KB2, and RPS6KA5 (Figure 5M and Table S1). Furthermore, we evaluated kinase activity upon a 5-min stimulation with soluble huCD19 protein for PTK analysis and upon a 20-min stimulation for STK analysis. Within the tested conditions, we observed strong changes in kinase activity on CAR6 cells compared to the signaling-deficient CAR5 cells, amplifying TK, CAMK, and AGC activity; specifically recruiting more TCR proximal kinases like SYK, JAK3, LYN, and ZAP70, which are linked to ITAM mediated signaling of the TCR/CD3 complex (reviewed in the studies by Darling et al., Hwang et al., and Shah et al.[24–26]) and CD16[27,28] (Figure 5N and Table S2). These results provide first line evidence on both tonic signaling and antigen-mediated signaling on CAR-NK cells.

Overall, CD3ζ SD tonic signaling introduced by CAR5 did not significantly impact the differentiation profile, phenotype and innate functionality of CD34$^+$ HSC-derived NK cells under tested conditions, whereas ITAMs in the CD3ζ SD have a vital role in mediating efficient antigen-specific activation of CAR-NK cells and targeting of tumor cells, functioning as cytotoxicity inducing "killer" domain.

CD28 TMD-containing CAR constructs show superior efficacy in kinetic *in vitro* assays using 3D tumor aggregates

To further investigate potential differences in the kinetics of the cytotoxicity of the two optimized CD28 TMD-containing CD19 CAR constructs (CAR2 and CAR4, Figure 4A) and CD3ζ TMD CAR1, we performed live cell imaging of CD19 CAR-NK cells in co-cultures with 3D aggregates of NALM-6 and Daudi over 48 h (Figure 6). CAR1, carrying the CD3ζ TMD, showed an antigen-specific capacity to control Daudi tumor aggregates at E:T 1:1 compared to Mock cells. Notably, CAR2 and CAR4, both containing the CD28 TMD, showed significantly higher capability for dissociation and eradication of the tumor aggregates compared to CAR1, however, no significant differences were seen between CAR2 and CAR4 (Figures 6A–6D and 6G). Interestingly, against 3D NALM-6 at 1:3 E:T, the three CAR constructs performed more similarly, with CAR4 being the fastest and most efficient leading to complete 3D aggregate eradication (Figures 6B–6E and 6H).

To further address the question of how much CAR$^+$ NK cells are needed to control tumor growth, we titrated down the proportion of CAR4 NK cells from 90% to 10% with Mock cells, and co-cultured them with NALM-6 cells that are minimally susceptible to unmodified NK cell killing at 1:3 E:T, thus using an adjusted actual CAR-NK:Target range of 1:3.3 (90% CAR) to 1:30 (10% CAR). We observed a dose-dependent cytotoxicity against the NALM-6 aggregates with a threshold of 20%, at which CAR-NK cells were no longer able to control tumor growth (Figures 6C–6F and 6I). Nevertheless, it is remarkable that CD34$^+$ HSC-derived CAR-NK cells can control 3D tumor growth as low as 1:15 (20% CAR) CAR-NK:Target ratio.

Figure 5. CD3ζ domain drives CAR-dependent cytotoxicity with a distinct tonic and antigen-mediated signaling profile while preserving natural cytotoxicity

(A) Schematic representation of cassette design for CARs 5 and 6.

(B) Percentage of CAR expression and (C) average CAR expression (ΔMFI) over 5 weeks post HSC transduction (MOI5) (n = 3 donors, two independent experiments).

(D) NK differentiation of transduced and Mock cells, starting from week 2 (n = 3 donors, two independent experiments).

(E) Representative dot plots of CAR expression at week 5 post-transduction. CAR positive cells, detected via G4S antibody, were pre-gated from the CD45$^+$/Viakrome808$^-$ cell population and plotted against CD56.

(F and G) CAR-NK and Mock cytotoxicity analysis assessed after 24 h via flow cytometry against (F) CD19$^+$ NALM-6 (E:T = 1:3) and (G) CD19$^-$ K562 (E:T = 1:1) (n = 3 donors, two independent experiments in technical triplicates).

(H–K) CAR-NK and Mock cytotoxicity analysis against 3D cell aggregates of (H) CD19$^+$ NLR-NALM-6 (E:T 1:4) or (J) NLR-Daudi (E:T 1:2) cells assessed over 48 h (n = 3 donors, two independent experiments in technical quadruplicates).

(I and K) Representative images of (I) NLR-NALM-6 and (K) NLR-Daudi aggregates at 10× magnification.

(L) Surface receptor expression profile of CAR-NK cells, analyzed on pre-gated CD3$^-$/CD14$^-$/CD15$^-$/CD19$^-$/CD56$^+$/Viakrome808$^-$/CAR$^+$ cells (n = 3 donors, two independent experiments). Top predicted upstream kinases analysis comparing CAR5 to CAR6 (M) at basal or (N) upon antigen stimulation visualized on the Coral kinome tree plot, where median final kinase score was used to group the kinases into phylogenetic families. Median final kinase score indicates a ranking based on the significance and specificity of the peptide set corresponding to a kinase ($p < 0.01$) (n = 3 donors). Data are shown as mean ± SD. Statistical analysis was performed using (F and G) One-way ANOVA with Sidak's multiple comparisons test and (M and N) two-sided Student's t test.

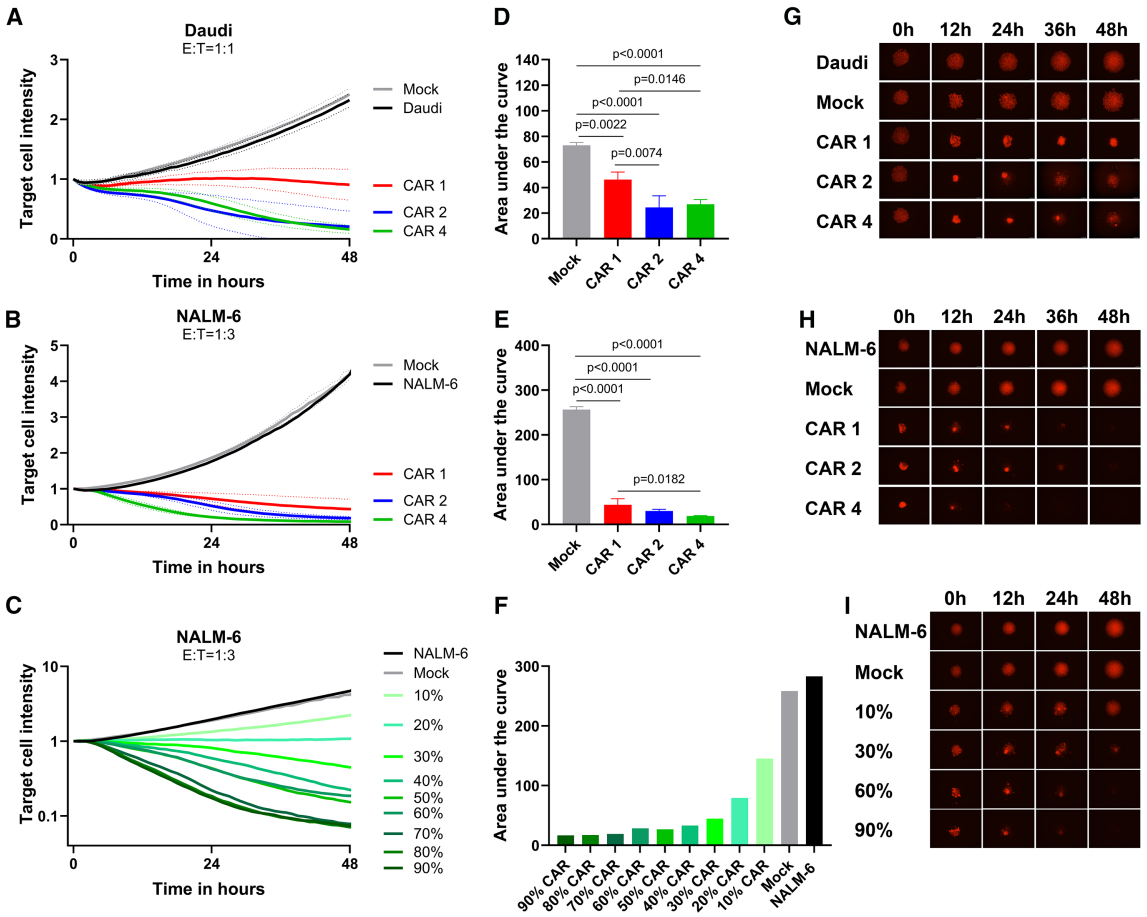

Figure 6. CD28 transmembrane domain mediates superior CAR-NK-mediated responses against 3D aggregates of highly or moderately-NK resistant tumor cell lines

(A–C) CAR-NK and Mock cytotoxicity assessed for 48 h against 3D aggregates of CD19$^+$ (A) NLR-Daudi (E:T = 1:1) or (B) NLR-NALM-6 (E:T = 1:3) (n = 3 donors, one independent experiment in technical quadruplicates), or (C) NLR-NALM-6 (E:T = 1:3) co-cultured with CAR4 diluted to a CAR$^+$ expression range of 90–10% (n = 1 donor, one independent experiment in technical quadruplicates).

(D–F) Area under the curve (D corresponding to A, E corresponding to B, and F corresponding to C), analyzed after 48 h (paired one-way ANOVA).

(G–I) Representative images of co-culture for (G) NLR-Daudi and (H and I) NLR-NALM-6 at 10× magnification captured at the indicated time points. Data are shown as mean ± SD.

(D and E) Statistical analysis was performed using one-way ANOVA with Tukey test.

CD28 transmembrane and co-stimulatory domains mediate sustained anti-tumor responses in repetitive *in vitro* 3D tumor assays and in an *in vivo* tumor model

Having seen that both CAR2 and CAR4, containing the CD28 TMD, were similar in their cytotoxic capacity to target CD19$^+$ tumor cells, even at more challenging 3D aggregate models, we developed a 3D repetitive challenge assay to further explore the persistence of the CAR-mediated cytotoxic response. The response was assessed over 3 rounds of new tumor exposure every 5–6 days using 3 donors expressing either CAR2 or CAR4 against NALM-6 3D aggregates (Figure 7A). While both designs efficiently eliminated NALM-6 3D aggregates in the first and second round of tumor exposure; in the third round, we observed a significant loss in tumor growth control capacity for CAR4, while CAR2 retained its functionality. This indicates a slightly improved efficacy advantage of CAR2 over CAR4, visualized in the representative images (Figure 7C). This phenomenon can partly be explained by the enhanced proliferation capacity and survival of CD28 SD containing CAR2 cells during the repetitive challenge assay, as increased numbers of CAR-NK cells were found after round 1, 2, and 3 for CAR2, while the cell counts for CAR4 were decreasing by each round (Figure 7B). Similar results supporting CAR2 advantage over CAR4 have been observed against CD19$^+$ Raji cells in an independent 2D repetitive challenge assay adapted from Acharya et al. (Figures S7A–S7F).[29] Although both CAR2 and CAR4 cells had pronounced cell proliferation capacities (Figures S7C and S7E), CAR2 cells had significantly higher tumor control capacity at both E:T ratio of 5:1 and 2:1 (Figures S7A and S7B).

Next, we compared the ability of the most potent CAR-NK candidates, CAR2 and CAR4, in controlling tumor growth *in vivo*. Survival and tumor growth was monitored for up to 30 days in a

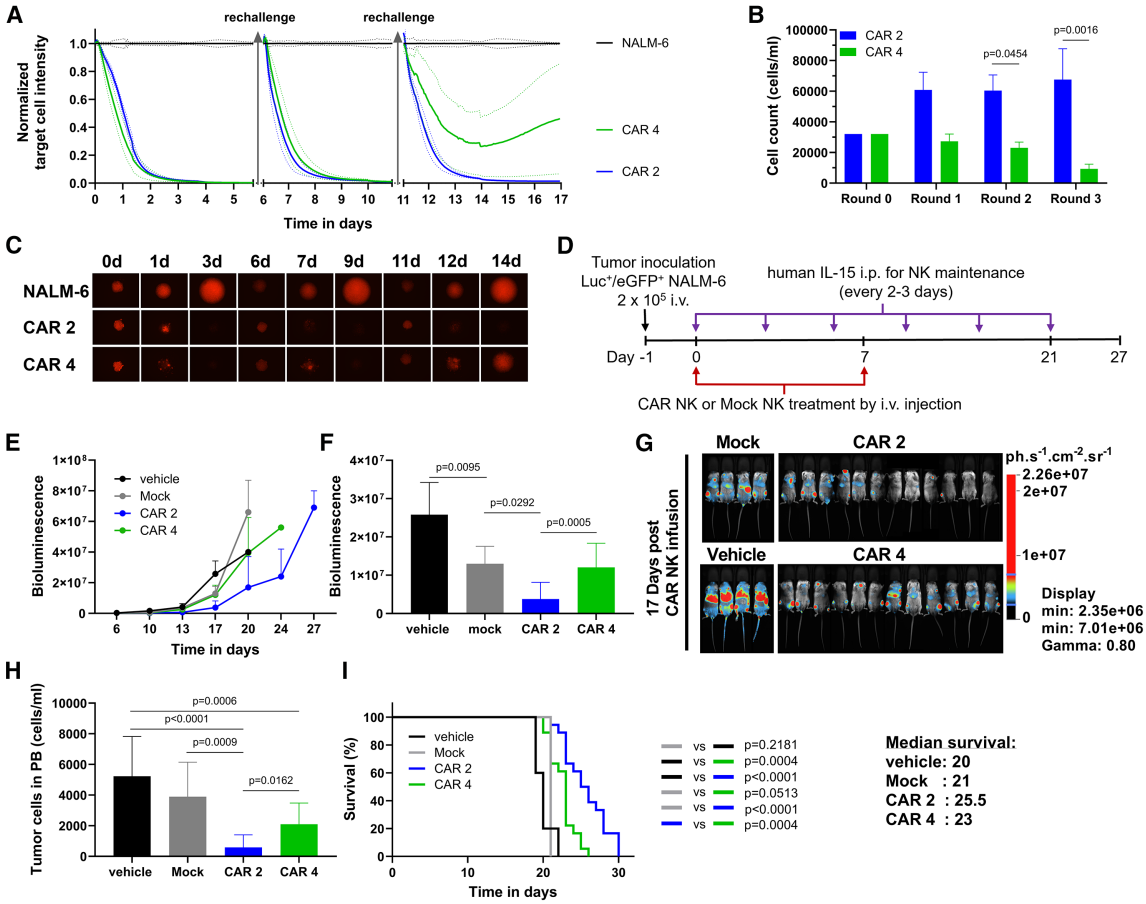

Figure 7. CD28 transmembrane and co-stimulatory domains lead to long-term tumor control in repetitive challenge assays and *in vivo*

(A) CAR-NK repetitive challenge cytotoxicity assay against 3D aggregates of CD19$^+$ NLR-NALM-6 (E:T = 1:1); after the first 6-day round, remaining cells were transferred to new aggregates for additional 5 days, then the same was repeated for the last round of 6 days (n = 3 donors, one independent experiment in technical quadruplicates). Mann-Whitney test showed a statistical difference of $p < 0.0001$ between CAR2 and CAR4.

(B) CAR-NK cell counts (cells/mL) measured at the end of each round (n = 3 donors).

(C) Representative images of indicated time points of co-culture of NALM-6 aggregates with one donor from one independent experiment are shown.

(D) Schematic outline of the NALM-6 *in vivo* study protocol. Tumor cells were intravenously (i.v.) administered at day −1. Mice received two intravenous (i.v.) Mock or CAR-NK cell injections and intraperitoneal (i.p.) human IL-15 injection every 2–3 days.

(E) *In vivo* bioluminescence intensity of Luc$^+$/eGFP$^+$ NALM-6 cells was monitored regularly for up to 27 days.

(F) *In vivo* bioluminescence intensity of Luc$^+$/eGFP$^+$ NALM-6 cells at day 17.

(G) Representative bioluminescence images on day 17.

(H) Circulating tumor cells measured in peripheral blood (PB) on day 14.

(I) Percentage of mice survival compared between groups until day 30.

(E–I) (n = 5 mice represented for vehicle, n = 4 mice for Mock donor, n = 18 mice for each CAR-NK construct). Data are shown as mean ± SD. Statistical analysis was performed using (B) two-way ANOVA with Tukey test (F–H) one-way ANOVA with Tukey test (I) Survival analysis was calculated using Kaplan-Meier methods and treatment groups were compared statistically using Log rank (Mantel-Cox) test with 95% confidence interval (CI).

very aggressive NALM-6 tumor model (Figure 7D). CAR-NK groups generally achieved better tumor control than Mock; notably, CAR2 showed higher efficacy than CAR4 (Figure 7E). The increased anti-tumor efficacy of CAR2 over CAR4 was evident on day 17, as shown by bioluminescence analysis and visualized in representative images throughout the duration of the study (Figures 7F and 7G, S8). Similar differences were observed by analyzing the circulating tumor cells in the peripheral blood of mice 14 days after treatment, where mice treated with CAR-NK cells showed significantly lower counts of NALM-6 cells than Mock, and even lower in CAR2 compared to CAR4 (Figure 7H). These findings are supported by survival analysis, with a higher median survival of 25.5 days for CAR2, compared to 23 days for CAR4 and 21 days for Mock (Figure 7I). The trend that was observed in the 3D repetitive challenge assay, where CD28 TMD, CD28 SD, and CD3ζ containing CAR2 showed better capacity to control tumor growth in the third round and increased proliferation capacity compared to CAR4, is also present in the mouse study, where CAR2 shows superior *in vivo* tumor control capacity compared to CAR4 highlighting the crucial role of CD28 SD domain in prolonged persistence of CAR-NK anti-tumor responses *in vitro* and *in vivo*.

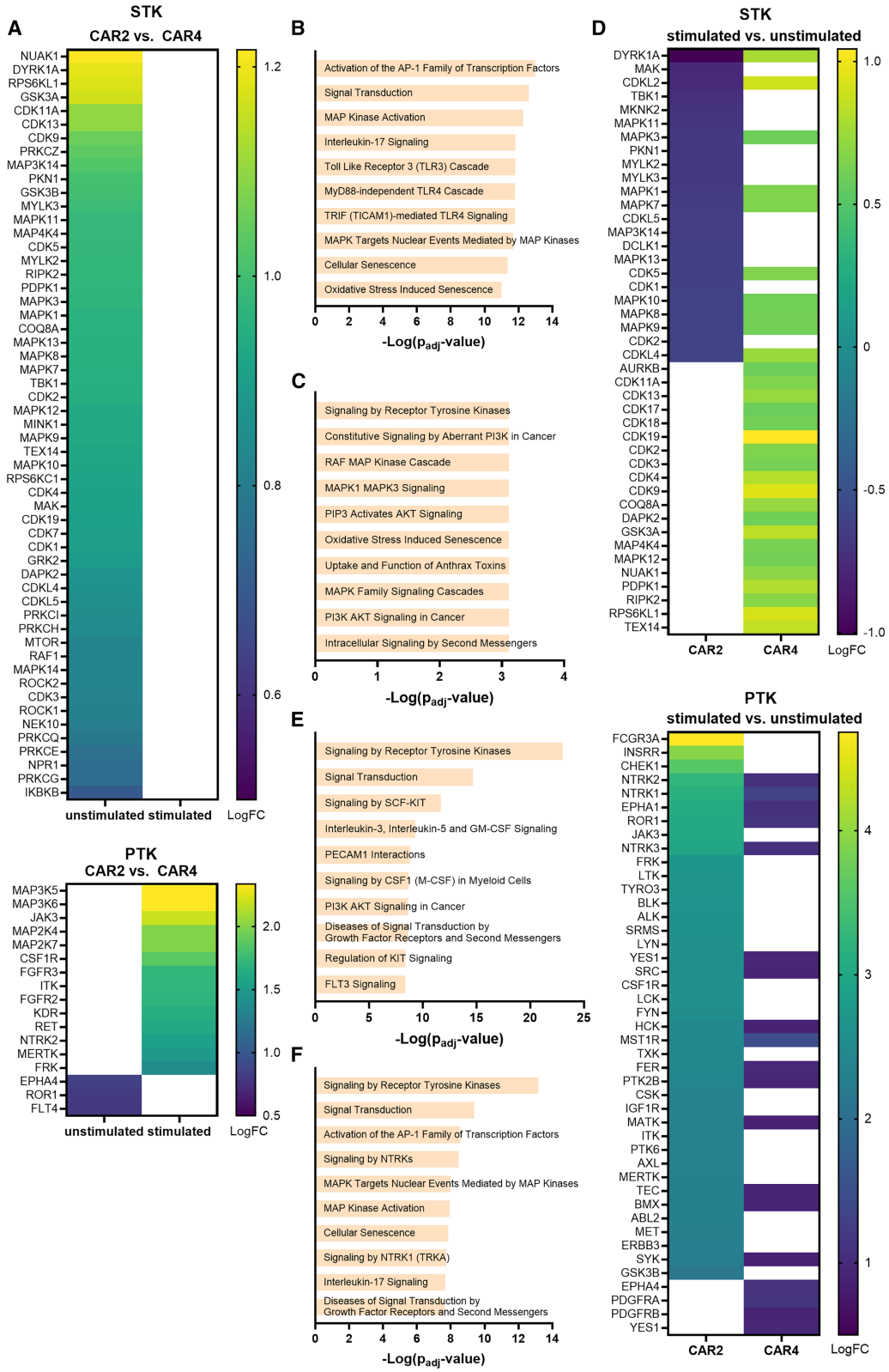

(legend on next page)

CD28 SD in CAR construct depicts a distinct kinome profile

Finally, to further portray the beneficial role of CD28 SD in tumor targeting and tumor growth control (Figure 7), we investigated the kinome profile of CAR2 and CAR4 with or without CD19 antigen stimulation (Figure 8). In unstimulated conditions, significant difference in kinase activity was observed between CAR2 and CAR4. Specifically, 59 out of 210 kinases showed higher activity in CAR2, while none showed lower activity. These kinases were mostly serine/threonine kinases (STKs), indicating differences in tonic signaling between CAR2 and CAR4. This finding suggests an important role for the CD28 SD domain even in the basal state (Figure 8A). Downstream pathway analysis revealed enrichment of pathways associated with cell proliferation and differentiation, such as "activation of the AP-1 family of transcription factors", "signal transduction", and "MAP kinase activation" in CAR2 compared to CAR4 (reviewed in the study by Karin et al., McKay et al., and Dong et al.[30–32]) (Figure 8B). Upon stimulation, CAR2 showed significantly higher kinome activity than CAR4 for 14 out of 210 kinases, all of which are receptor TK (PTKs) responsible for the regulation of many cellular processes, including pathways like "signaling by receptor TK," "aberrant PI3K signaling in cancer," and "RAF MAP kinase cascade" (Figures 8A and 8C). Enhanced activation in CAR2 was also evident by the enrichment of TCR-related kinases,[33–35] such as LYN, LCK, SRC, FYN, HCK, and SYK, observed in stimulated vs. unstimulated conditions (Figure 8D). These kinases also play a crucial role in NK activation and cytotoxicity.[35] Additionally, CAR2 exhibited increased activity in pathways linked to proliferation, such as "signaling by SCF-KIT" (Figure 8E). Interestingly, antigen stimulation in CAR2 led to a decrease in STK activity, which was not observed in CAR4. Basal STK activity in CAR2 was also substantially higher than in CAR4 (Figures 8A and 8D). In CAR4, antigen stimulation also increased PTK activity, linked to pathways like "signaling by receptor TK" and "signal transduction," but the extent of activation was lower than in CAR2 (Figure 8F). Overall, in line with the observed beneficial role of the CD28 SD in tumor targeting and tumor growth control (Figure 7), the differences in kinome profiles suggest that CAR2 exhibits stronger basal and antigen-induced kinase activity, likely due to the CD28 SD domain, leading to enhanced tonic signaling as well as proliferation and signaling upon CD19 stimulation.

DISCUSSION

In this study we aimed to provide a comprehensive understanding on optimization of CAR cassettes for efficient and persistent anti-tumor responses using HSCs as start material in a clinical compatible research grade stem cell expansion and NK cell differentiation platform[21,22]. To our knowledge, this is the first study on feeder cell-free HSC-derived NK cells that comparatively investigates the role of different promoters, hinges, TMDs, and SDs in CAR-expression and CAR-mediated antigen-specific targeting of tumor cells, using the well-established CD19-specific scFv (FMC63).[36] Our data show that for UCB-derived NK cells, the use of the MNDU3 promoter, CD8α hinge, CD28 TMD and CD28 SD and CD3ζ SD, facilitated high and stable CAR expression throughout the expansion and differentiation phase and demonstrated significantly improved and sustained cytotoxicity compared to other construct designs. We also profiled CD3ζ SD kinase activity of UCB-derived NK cells providing essential information about tonic and antigen-mediated signaling of CAR-NK cells expanding the knowledge regarding kinome profile of NK cells at steady state and under antigen stimulation.[27]

These results align with existing NK-cell literature that supports the robustness of the MNDU3 promoter, also referred to as myeloproliferative sarcoma virus (MPSV) fused with U3, in maintaining high levels of CAR transgene expression, which is crucial for long-term antitumor activity.[19,37,38] In our hands, the combination of 4-1BB TMD and SD with CD3ζ SD, as a second-generation CAR, negatively affected transduction rates and did not achieve stable CAR expression on NK-92 cells. Recent studies on NK-92 cells comparing constructs containing CD28 TMD/SD and 4-1BB TMD/SD plus CD3ζ SD also confirm that the combination with 4-1BB TMD/SD is not always the best choice.[39,40] Similarly, a strong decrease in CAR^+ cells two weeks post transduction of $CD34^+$ HSCs was observed, suggesting a selective depletion/elimination of CAR^+ cells potentially due to tonic 4-1BB signaling. In line with this observation, Choi et al. reported that 4-1BB signaling has been linked to a less favorable impact on stem cells and progenitors, suppressing NK-cell hematopoiesis, and differentiation through 4-1BB triggered production of IFN-γ from T cells and NK cells.[41]

On the other hand, the CD28 co-stimulatory molecule has a significant role in T cell activation as well as survival and both TMD and SD derived from CD28 have been evaluated in multiple preclinical and clinical CAR-T cell studies.[42] Improved *in vivo* T cell expansion, persistence and tumor control, compared to first generation CAR cassettes, are associated with the use of CD28 SD in CAR-T cells.[42] Likewise, benefits of having CD28 SD are also reported for CAR-NK cells with limited comparative analysis of multiple components of the CAR cassettes except in studies performed on NK-92 cells.[2] However, there is limited information on the direct role of CD28 on NK cell development and function. Expression of

Figure 8. CD28 SD exhibits stronger tonic and antigen-induced kinase activity

(A) Log_2-Fold changes of the kinases identified by comparing CAR2 vs. CAR4 in unstimulated and stimulated condition with median final score >1.3 and $Log_2FC > 0.58$, distinguished as STK (serine/threonine) or PTK (protein tyrosine) kinases.

(B and C) The top 10 enriched pathways for the input kinase set comparing (B) CAR2 vs. CAR4 in the unstimulated condition and (C) CAR2 vs. CAR4 in the stimulated condition are displayed based on the -log10(p_{adj}-value).

(D) Log_2-Fold changes of the kinases identified by comparing stimulated vs. unstimulated in CAR2 and CAR4 with median final score >1.3 and $Log_2FC > 0.58$, separated by STK and PTK kinases.

(E and F) The top 10 enriched pathways for the input kinase set comparing (E) stimulated vs. unstimulated in CAR2 and (F) stimulated vs. unstimulated in CAR4 are displayed based on the -log10(p_{adj}-value). Statistical analysis was performed using two-sided Student's t test ($p < 0.05$).

CD28, and its homolog CD28H, has been demonstrated on activated PB-NK cells and NK cell lines and expression of CD28H on PB-NK cells has shown to induce synergistic effects with the activation receptors NKp46 and 2B4 to initiate NK cell degranulation and cytotoxicity, as well as enhanced CD16-mediated ADCC.[43] Nevertheless, comparable NK cell development in CD28 k/o mice has been observed and our previous studies demonstrated that CD28 is hardly expressed throughout NK cell differentiation.[44] Collectively, for HSC-derived NK cells, here we demonstrated that CD28 SD significantly contributes to (1) enhanced *ex vivo* CD16 expression despite the reports on low/no CD16 expression on stem cell derived NK cells especially cultured without feeder cells[3,45], (2) faster NK cell differentiation and early maturation, (3) CAR expression stability on $CD34^+$ HSC-derived NK cells, and (4) prolonged persistence and tumor antigen-induced CAR-NK proliferation through (5) switching on additional activating signaling pathways that are otherwise inaccessible in the absence of CD28 expression in the context of feeder-free *ex vivo* NK cell hematopoiesis and function. Interestingly, in a recent study investigating the influence of costimulatory domains CD28, 4-1BB, DAP10, DAP12, and CD3ζ SD in combination with CD28 TMD in CD70-targeting CAR transduced UCB-NK cells.[29] This study showed that the inclusion of CD28 costimulatory domain significantly improved persistence and sustained cytotoxicity by recruiting lymphocyte-specific PTK (LCK) leading to phosphorylation of CD3ζ and recruitment and autophosphorylation of the CD3ζ-chain-associated protein kinase 70 (ZAP70) and initiating downstream signaling such as the AKT pathway.[29] In line with this recently published data on already differentiated UCB-NK cells, our functional data and high resolution kinome profiling further supports the incorporation of CD28 TMD and SD as a very promising component for $CD34^+$ HSC-derived CAR-NK cell generation and further enhances the understanding on the role of CD28 SD on *ex vivo* NK differentiation and maturation even though CD28 is not tightly associated with NK cell development and function.

In conclusion, in this study we evaluated the role of different CAR-cassette components on HSC-derived NK cells using CD19 as model. Further enhancement of *in vivo* performance of $CD34^+$ HSC-derived CAR-NK cells can be achieved (1) via incorporation of cytokine genes such as IL-15 or IL-21, which could enhance the proliferation and persistence of CAR-NK cells *in vivo* and thereby improving the long lasting anti-tumor responses, as was observed by others[46,47]; (2) engineering CAR-NK cells to resist immunosuppressive signals from the tumor microenvironment (TME) could significantly improve their therapeutic efficacy by modifying cells to express dominant-negative receptors or mechanisms to counteract TGF-β, PD-L1, or other inhibitory signals[48]; (3) NK-specific transmembrane and signaling domains to further tailor CAR constructs to NK cell biology and enhance antitumor activity can also be explored[49]; (4) additionally, integrating CAR-NK cell therapy with other immunotherapies, such as checkpoint inhibitors or bispecific antibodies, could produce synergistic effects, leading to improved treatment outcomes.[50,51] Altogether, the results of this study and its potential to facilitate future modifications aiming to enhance *in vivo* efficacy and persistence of CAR-NK cells, address key gaps in knowledge and pave the way for developing safer and more effective CAR-NK cell therapies for hematologic malignancies and solid tumors, as well as autoimmune diseases.

Limitations of the study

The diversity of CAR-NK studies in terms of cell sources and methods used to generate and culture CAR-NK cells, as well as the antigenic targets and experimental models used to verify the results constitute major limitations in the field. Moreover, it is difficult to fully comprehend the specific construct design of each CAR used in CAR-NK studies, and in our experience learnings from NK cell lines or primary NK cell-based studies can be misleading for developing stem cell-derived NK cell-based therapies. Furthermore, differences in cytokine cocktails, media, time etc. can still impact the experimental outcomes highlighting the importance of source-specific screening and optimizations when it comes to future CAR-NK manufacturing.[38] Moreover, the paramount importance of safety in the development of genetically engineered cell products, particularly those derived from stem cells, requires further preclinical and clinical risk evaluation of LV backbones, promoters, LV insertion sites etc. In fact, insertional mutagenesis is a risk not only for $CD34^+$ stem cell products, but also for CAR-T cell products. A recent report on the GM autologous stem cell product elivaldogene autotemcel (eli-cel) showed that hematological cancer (AML or MDS) developed in 7 out of 67 patients after eli-cel administration, which is potentially associated with clonal vector insertions within oncogenes and potentially with pre-existing or evolving somatic mutations.[52] It is important to note that the MNDU3 promoter was used in the LV vector but no direct association to observe tumorigenicity was reported. In our case, this risk is significantly minimized as (1) allogeneic NK cells generally persist during a short period of time and will be rejected once the patient's immune system has recovered from the lymphodepleting preconditioning. However, it is still possible to see CAR-NK cell *in vivo* persistence up to a year when supported by ectopic IL-15 expression[53] (2) more than 90% of the cells at the end of the process are NK cells, (3) our platform facilitates efficient genetic modification below VCN 5 as suggested by WHO communication for lentiviral vector integration,[54,55] and (4) recent single-cell analysis of our NK cell product revealed no expression of stem cell markers such as CD34, CD133 (PROM1), CD90 (THY1), CD49f (ITGA6), and EPCR (PROCR).[56] Finally, specifically for this study, our conclusions are mainly based on the FMC63 clone and a limited set of B cell malignancy cells lines. Therefore, use and evaluation of different CAR components, such as promoters, hinges, SDs or further modifications might be necessary for other scFv, targets, and indications.

RESOURCE AVAILABILITY

Lead contact

Further information and requests for resources and reagents should be directed to and will be fulfilled by the lead contact, Adil D. Duru (adil@glycostem.com).

Materials availability

This study did not generate new unique reagents.

Data and code availability

- All data reported in this paper will be shared by the lead contact upon request.
- This paper does not report original code.
- Any additional information required to reanalyze the data reported in this paper is available from the lead contact upon request.

ACKNOWLEDGMENTS

We would like to thank Simone Mantesso, Josephine Stein, Youri van Waardenburg, Denise Panella, Denise Vodegel, Arianna Miccichè, Esther van der End, Daan de Bruijckere, and Angela Bella Carreño for their work supporting this study. We would also like to thank Gitanjali Dharmadhikari and Dirk Pijnenburg from PamGene International B.V. for their support. This study is funded by Glycostem Therapeutics B.V. Graphical abstract was created with BioRender.com.

AUTHOR CONTRIBUTIONS

A.D.D. and J.S. conceptualized the study. A.D.D., J.S., M.R. and A.-M.G. designed the research study. A.A.v.V. and T.S. provided technical expertise. N.K., D.O., A.A.v.V., and D.S. performed experiments, analyzed and/or interpreted the data. S.P.S., A.-M.G. and A.D.D. designed the kinome mapping study. N.K., D.O., A.A.v.V., A.-M.G., M.R., J.S., and A.D.D. wrote the manuscript.

DECLARATION OF INTERESTS

N.K., D.O., D.S., A.A.v.V., A.-M.G., M.R., J.S., and A.D.D. are employees of Glycostem Therapeutics. Glycostem Therapeutics B.V. holds patent applications related to this work. N.K., M.R., and J.S. are employees of Glycostem Therapeutics B.V. and are mentioned as inventors on the following related international patent applications: PCT/EP2019/063920, PCT/NL2020/050478, and PCT/NL2020/050745, and on national patent applications derived therefrom. A.D.D. and T.S. are shareholders in Vycellix Inc. T.S. holds a consulting position in Epsilon Elektronik. S.P.S. is an employee of PamGene International B.V.

STAR★METHODS

Detailed methods are provided in the online version of this paper and include the following:

- KEY RESOURCES TABLE
- EXPERIMENTAL MODEL AND STUDY PARTICIPANT
  - Ethics statement
- CELL LINES
- *IN VIVO* ANIMAL STUDIES
- METHOD DETAILS
  - Cell lines
  - GS lentiviral plasmid backbone construction and CAR cassette design
  - Lentiviral vector production and titer determination
  - Lentiviral transduction of NK-92 cells
  - Lentiviral transduction of UCB-derived primary $CD34^+$ cells for CAR-NK generation
  - Cryopreservation of CAR-NK cells
  - Genomic DNA isolation and vector copy number determination by quantitative PCR
  - *In vitro* 24h flow cytometry-based cytotoxicity and 5h cytotoxicity/degranulation assay
  - Assessment of intracellular expression of IFN-γ, TNF, perforin or Granzyme B
  - Phenotypic characterization of CAR-NK cells
  - Protein kinase activity profiling using PamChip peptide microarrays
  - Incucyte live cell cytotoxicity assays
  - Tumor xenograft mouse model
- QUANTIFICATION AND STATISTICAL ANALYSIS

SUPPLEMENTAL INFORMATION

Supplemental information can be found online at https://doi.org/10.1016/j.isci.2025.112548.

Received: September 24, 2024
Revised: December 20, 2024
Accepted: April 25, 2025
Published: April 29, 2025

REFERENCES

1. Cappell, K.M., and Kochenderfer, J.N. (2023). Long-term outcomes following CAR T cell therapy: what we know so far. Nat. Rev. Clin. Oncol. *20*, 359–371.
2. Lamers-Kok, N., Panella, D., Georgoudaki, A.M., Liu, H., Özkazanc, D., Kučerová, L., Duru, A.D., Spanholtz, J., and Raimo, M. (2022). Natural killer cells in clinical development as non-engineered, engineered, and combination therapies. J. Hematol. Oncol. *15*, 164.
3. Dolstra, H., Roeven, M.W.H., Spanholtz, J., Hangalapura, B.N., Tordoir, M., Maas, F., Leenders, M., Bohme, F., Kok, N., Trilsbeek, C., et al. (2017). Successful Transfer of Umbilical Cord Blood CD34(+) Hematopoietic Stem and Progenitor-derived NK Cells in Older Acute Myeloid Leukemia Patients. Clin. Cancer Res. *23*, 4107–4118.
4. Mantesso, S., Geerts, D., Spanholtz, J., and Kučerová, L. (2020). Genetic Engineering of Natural Killer Cells for Enhanced Antitumor Function. Front. Immunol. *11*, 607131.
5. Sutlu, T., Nyström, S., Gilljam, M., Stellan, B., Applequist, S.E., and Alici, E. (2012). Inhibition of intracellular antiviral defense mechanisms augments lentiviral transduction of human natural killer cells: implications for gene therapy. Hum. Gene Ther. *23*, 1090–1100.
6. Maia, A., Tarannum, M., and Romee, R. (2024). Genetic Manipulation Approaches to Enhance the Clinical Application of NK Cell-Based Immunotherapy. Stem Cells Transl. Med. *13*, 230–242.
7. Allan, D.S.J., Chakraborty, M., Waller, G.C., Hochman, M.J., Poolcharoen, A., Reger, R.N., and Childs, R.W. (2021). Systematic improvements in lentiviral transduction of primary human natural killer cells undergoing ex vivo expansion. Mol. Ther. Methods Clin. Dev. *20*, 559–571.
8. Page, A., Chuvin, N., Valladeau-Guilemond, J., and Depil, S. (2024). Development of NK cell-based cancer immunotherapies through receptor engineering. Cell. Mol. Immunol. *21*, 315–331.
9. Gong, Y., Klein Wolterink, R.G.J., Wang, J., Bos, G.M.J., and Germeraad, W.T.V. (2021). Chimeric antigen receptor natural killer (CAR-NK) cell design and engineering for cancer therapy. J. Hematol. Oncol. *14*, 73.
10. Cao, B., Liu, M., Huang, J., Zhou, J., Li, J., Lian, H., Huang, W., Guo, Y., Yang, S., Lin, L., et al. (2021). Development of mesothelin-specific CAR NK-92 cells for the treatment of gastric cancer. Int. J. Biol. Sci. *17*, 3850–3861.
11. Lu, C., Guo, C., Chen, H., Zhang, H., Zhi, L., Lv, T., Li, M., Niu, Z., Lu, P., and Zhu, W. (2020). A novel chimeric PD1-NKG2D-41BB receptor enhances antitumor activity of NK92 cells against human lung cancer H1299 cells by triggering pyroptosis. Mol. Immunol. *122*, 200–206.
12. Xiao, L., Cen, D., Gan, H., Sun, Y., Huang, N., Xiong, H., Jin, Q., Su, L., Liu, X., Wang, K., et al. (2019). Adoptive Transfer of NKG2D CAR mRNA-Engineered Natural Killer Cells in Colorectal Cancer Patients. Mol. Ther. *27*, 1114–1125.
13. Chang, Y.H., Connolly, J., Shimasaki, N., Mimura, K., Kono, K., and Campana, D. (2013). A chimeric receptor with NKG2D specificity enhances natural killer cell activation and killing of tumor cells. Cancer Res. *73*, 1777–1786.
14. Topfer, K., Cartellieri, M., Michen, S., Wiedemuth, R., Müller, N., Lindemann, D., Bachmann, M., Füssel, M., Schackert, G., and Temme, A. (2015). DAP12-based activating chimeric antigen receptor for NK cell tumor immunotherapy. J. Immunol. *194*, 3201–3212.

15. Ao, X., Yang, Y., Li, W., Tan, Y., Guo, W., Ao, L., He, X., Wu, X., Xia, J., Xu, X., and Guo, J. (2019). Anti-alphaFR CAR-engineered NK-92 Cells Display Potent Cytotoxicity Against alphaFR-positive Ovarian Cancer. J. Immunother. *42*, 284–296.

16. Li, Y., Hermanson, D.L., Moriarity, B.S., and Kaufman, D.S. (2018). Human iPSC-Derived Natural Killer Cells Engineered with Chimeric Antigen Receptors Enhance Anti-tumor Activity. Cell Stem Cell *23*, 181–192.

17. Mansour, A.G., Teng, K.Y., Li, Z., Zhu, Z., Chen, H., Tian, L., Ali, A., Zhang, J., Lu, T., Ma, S., et al. (2023). Off-the-shelf CAR-engineered natural killer cells targeting FLT3 enhance killing of acute myeloid leukemia. Blood Adv. *7*, 6225–6239.

18. Liu, W.N., So, W.Y., Harden, S.L., Fong, S.Y., Wong, M.X.Y., Tan, W.W.S., Tan, S.Y., Ong, J.K.L., Rajarethinam, R., Liu, M., et al. (2022). Successful targeting of PD-1/PD-L1 with chimeric antigen receptor-natural killer cells and nivolumab in a humanized mouse cancer model. Sci. Adv. *8*, eadd1187.

19. De Oliveira, S.N., Ryan, C., Giannoni, F., Hardee, C.L., Tremcinska, I., Katebian, B., Wherley, J., Sahaghian, A., Tu, A., Grogan, T., et al. (2013). Modification of hematopoietic stem/progenitor cells with CD19-specific chimeric antigen receptors as a novel approach for cancer immunotherapy. Hum. Gene Ther. *24*, 824–839.

20. Wen, W., Chen, X., Shen, X.Y., Li, H.Y., Zhang, F., Fang, F.Q., and Zhang, X.B. (2023). Enhancing cord blood stem cell-derived NK cell growth and differentiation through hyperosmosis. Stem Cell Res. Ther. *14*, 295.

21. Spanholtz, J., Tordoir, M., Eissens, D., Preijers, F., van der Meer, A., Joosten, I., Schaap, N., de Witte, T.M., and Dolstra, H. (2010). High log-scale expansion of functional human natural killer cells from umbilical cord blood CD34-positive cells for adoptive cancer immunotherapy. PLoS One *5*, e9221.

22. Spanholtz, J., Preijers, F., Tordoir, M., Trilsbeek, C., Paardekooper, J., de Witte, T., Schaap, N., and Dolstra, H. (2011). Clinical-grade generation of active NK cells from cord blood hematopoietic progenitor cells for immunotherapy using a closed-system culture process. PLoS One *6*, e20740.

23. Schindler, K., Eva Ruppel, K., Müller, C., Koehl, U., Fricke, S., and Schmiedel, D. (2024). Linker-specific monoclonal antibodies present a simple and reliable detection method for scFv-based CARNK cells. Mol. Ther. *32*, 3101328.

24. Darling, T.K., and Lamb, T.J. (2019). Emerging Roles for Eph Receptors and Ephrin Ligands in Immunity. Front. Immunol. *10*, 1473.

25. Hwang, J.R., Byeon, Y., Kim, D., and Park, S.G. (2020). Recent insights of T cell receptor-mediated signaling pathways for T cell activation and development. Exp. Mol. Med. *52*, 750–761.

26. Shah, K., Al-Haidari, A., Sun, J., and Kazi, J.U. (2021). T cell receptor (TCR) signaling in health and disease. Signal Transduct. Target. Ther. *6*, 412.

27. Konig, S., Nimtz, M., Scheiter, M., Ljunggren, H.G., Bryceson, Y.T., and Jänsch, L. (2012). Kinome analysis of receptor-induced phosphorylation in human natural killer cells. PLoS One *7*, e29672.

28. Mkaddem, S.B., Murua, A., Flament, H., Titeca-Beauport, D., Bounaix, C., Danelli, L., Launay, P., Benhamou, M., Blank, U., Daugas, E., et al. (2017). Lyn and Fyn function as molecular switches that control immunoreceptors to direct homeostasis or inflammation. Nat. Commun. *8*, 246.

29. Acharya, S., Acharya, S., Basar, R., Daher, M., Rafei, H., Li, P., Uprety, N., Ensley, E., Shanley, M., Kumar, B., and Banerjee, P.P. (2024). CD28 costimulation augments CAR signaling in NK cells via the LCK/CD3Z/ZAP70 signaling axis. Cancer Discov. *140*, 1879–1900.

30. Karin, M., Liu, Z.g., and Zandi, E. (1997). AP-1 function and regulation. Curr. Opin. Cell Biol. *9*, 240–246.

31. McKay, M.M., and Morrison, D.K. (2007). Integrating signals from RTKs to ERK/MAPK. Oncogene *26*, 3113–3121.

32. Dong, C., Davis, R.J., and Flavell, R.A. (2002). MAP kinases in the immune response. Annu. Rev. Immunol. *20*, 55–72.

33. Krebs, D.L., Chehal, M.K., Sio, A., Huntington, N.D., Da, M.L., Ziltener, P., Inglese, M., Kountouri, N., Priatel, J.J., Jones, J., et al. (2012). Lyn-dependent signaling regulates the innate immune response by controlling dendritic cell activation of NK cells. J. Immunol. *188*, 5094–5105.

34. Lowin-Kropf, B., Kunz, B., Schneider, P., and Held, W. (2002). A role for the src family kinase Fyn in NK cell activation and the formation of the repertoire of Ly49 receptors. Eur. J. Immunol. *32*, 773–782.

35. Brumbaugh, K.M., Binstadt, B.A., Billadeau, D.D., Schoon, R.A., Dick, C. J., Ten, R.M., and Leibson, P.J. (1997). Functional role for Syk tyrosine kinase in natural killer cell-mediated natural cytotoxicity. J. Exp. Med. *186*, 1965–1974.

36. Zola, H., MacArdle, P.J., Bradford, T., Weedon, H., Yasui, H., and Kurosawa, Y. (1991). Preparation and characterization of a chimeric CD19 monoclonal antibody. Immunol. Cell Biol. *69*, 411–422.

37. Lowe, E., Truscott, L.C., and De Oliveira, S.N. (2016). In Vitro Generation of Human NK Cells Expressing Chimeric Antigen Receptor Through Differentiation of Gene-Modified Hematopoietic Stem Cells. Methods Mol. Biol. *1441*, 241–251.

38. Ho, J.Y., Wang, L., Liu, Y., Ba, M., Yang, J., Zhang, X., Chen, D., Lu, P., and Li, J. (2021). Promoter usage regulating the surface density of CAR molecules may modulate the kinetics of CAR-T cells in vivo. Mol. Ther. Methods Clin. Dev. *21*, 237–246.

39. Oelsner, S., Friede, M.E., Zhang, C., Wagner, J., Badura, S., Bader, P., Ullrich, E., Ottmann, O.G., Klingemann, H., Tonn, T., and Wels, W.S. (2017). Continuously expanding CAR NK-92 cells display selective cytotoxicity against B-cell leukemia and lymphoma. Cytotherapy *19*, 235–249.

40. Schonfeld, K., Sahm, C., Zhang, C., Naundorf, S., Brendel, C., Odendahl, M., Nowakowska, P., Bönig, H., Köhl, U., Kloess, S., et al. (2015). Selective inhibition of tumor growth by clonal NK cells expressing an ErbB2/HER2-specific chimeric antigen receptor. Mol. Ther. *23*, 330–338.

41. Choi, B.K., Kim, Y.H., Kim, C.H., Kim, M.S., Kim, K.H., Oh, H.S., Lee, M.J., Lee, D.K., Vinay, D.S., and Kwon, B.S. (2010). Peripheral 4-1BB signaling negatively regulates NK cell development through IFN-gamma. J. Immunol. *185*, 1404–1411.

42. Smith, R., and Shen, R. (2023). Complexities in comparing the impact of costimulatory domains on approved CD19 CAR functionality. J. Transl. Med. *21*, 515.

43. Zhuang, X., and Long, E.O. (2019). CD28 Homolog Is a Strong Activator of Natural Killer Cells for Lysis of B7H7(+) Tumor Cells. Cancer Immunol. Res. *7*, 939–951.

44. Lehmann, D., Spanholtz, J., Osl, M., Tordoir, M., Lipnik, K., Bilban, M., Schlechta, B., Dolstra, H., and Hofer, E. (2012). Ex vivo generated natural killer cells acquire typical natural killer receptors and display a cytotoxic gene expression profile similar to peripheral blood natural killer cells. Stem Cells Dev. *21*, 2926–2938.

45. Kang, L., Voskinarian-Berse, V., Law, E., Reddin, T., Bhatia, M., Hariri, A., Ning, Y., Dong, D., Maguire, T., Yarmush, M., et al. (2013). Characterization and ex vivo Expansion of Human Placenta-Derived Natural Killer Cells for Cancer Immunotherapy. Front. Immunol. *4*, 101.

46. Li, L., Mohanty, V., Dou, J., Huang, Y., Banerjee, P.P., Miao, Q., Lohr, J.G., Vijaykumar, T., Frede, J., Knoechel, B., et al. (2023). Loss of metabolic fitness drives tumor resistance after CAR-NK cell therapy and can be overcome by cytokine engineering. Sci. Adv. *9*, eadd6997.

47. Zhang, Y., Zhang, C., He, M., Xing, W., Hou, R., and Zhang, H. (2024). Co-expression of IL-21-Enhanced NKG2D CAR-NK cell therapy for lung cancer. BMC Cancer *24*, 119.

48. Valeri, A., García-Ortiz, A., Castellano, E., Córdoba, L., Maroto-Martín, E., Encinas, J., Leivas, A., Río, P., and Martínez-López, J. (2022). Overcoming tumor resistance mechanisms in CAR-NK cell therapy. Front. Immunol. *13*, 953849.

49. Imai, C., Iwamoto, S., and Campana, D. (2005). Genetic modification of primary natural killer cells overcomes inhibitory signals and induces specific killing of leukemic cells. Blood *106*, 376–383.

50. Kong, X., Zhang, J., Chen, S., Wang, X., Xi, Q., Shen, H., and Zhang, R. (2024). Immune checkpoint inhibitors: breakthroughs in cancer treatment. Cancer Biol. Med. *21*, 451–472.

51. Trabolsi, A., Arumov, A., and Schatz, J.H. (2024). Bispecific antibodies and CAR-T cells: dueling immunotherapies for large B-cell lymphomas. Blood Cancer J. *14*, 27.

52. Duncan, C.N., Bledsoe, J.R., Grzywacz, B., Beckman, A., Bonner, M., Eichler, F.S., Kühl, J.S., Harris, M.H., Slauson, S., Colvin, R.A., et al. (2024). Hematologic Cancer after Gene Therapy for Cerebral Adrenoleukodystrophy. N. Engl. J. Med. *391*, 1287–1301.

53. Marin, D., Li, Y., Basar, R., Rafei, H., Daher, M., Dou, J., Mohanty, V., Dede, M., Nieto, Y., Uprety, N., et al. (2024). Safety, efficacy and determinants of response of allogeneic CD19-specific CAR-NK cells in CD19(+) B cell tumors: a phase 1/2 trial. Nat. Med. *30*, 772–784.

54. Organization, W.H. (2019). WHO-BS-2019.2373 (World Health Organization).

55. Zhao, Y., Stepto, H., and Schneider, C.K. (2017). Development of the First World Health Organization Lentiviral Vector Standard: Toward the Production Control and Standardization of Lentivirus-Based Gene Therapy Products. Hum. Gene Ther. Methods *28*, 205–214.

56. van Vliet, A.A., van den Hout, M.G.C.N., Steenmans, D., Duru, A.D., Georgoudaki, A.M., de Gruijl, T.D., van IJcken, W.F.J., Spanholtz, J., and Raimo, M. (2024). Bulk and single-cell transcriptomics identify gene signatures of stem cell-derived NK cell donors with superior cytolytic activity. Mol. Ther. Oncol. *32*, 200870.

57. Larionov, A., Krause, A., and Miller, W. (2005). A standard curve based method for relative real time PCR data processing. BMC Bioinf. *6*, 62.

58. van Vliet, A.A., Peters, E., Vodegel, D., Steenmans, D., Raimo, M., Gibbs, S., de Gruijl, T.D., Duru, A.D., Spanholtz, J., and Georgoudaki, A.M. (2023). Early TRAIL-engagement elicits potent multimodal targeting of melanoma by CD34(+) progenitor cell-derived NK cells. iScience *26*, 107078.

59. Wang, J., Pollard, K., Allen, A.N., Tomar, T., Pijnenburg, D., Yao, Z., Rodriguez, F.J., and Pratilas, C.A. (2020). Combined Inhibition of SHP2 and MEK Is Effective in Models of NF1-Deficient Malignant Peripheral Nerve Sheath Tumors. Cancer Res. *80*, 5367–5379.

60. Manning, G., Whyte, D.B., Martinez, R., Hunter, T., and Sudarsanam, S. (2002). The protein kinase complement of the human genome. Science *298*, 1912–1934.

61. Chen, E.Y., Tan, C.M., Kou, Y., Duan, Q., Wang, Z., Meirelles, G.V., Clark, N.R., and Ma'ayan, A. (2013). Enrichr: interactive and collaborative HTML5 gene list enrichment analysis tool. BMC Bioinf. *14*, 128.

62. Xie, Z., Bailey, A., Kuleshov, M.V., Clarke, D.J.B., Evangelista, J.E., Jenkins, S.L., Lachmann, A., Wojciechowicz, M.L., Kropiwnicki, E., Jagodnik, K.M., et al. (2021). Gene Set Knowledge Discovery with Enrichr. Curr. Protoc. *1*, e90.

63. Kuleshov, M.V., Jones, M.R., Rouillard, A.D., Fernandez, N.F., Duan, Q., Wang, Z., Koplev, S., Jenkins, S.L., Jagodnik, K.M., Lachmann, A., et al. (2016). Enrichr: a comprehensive gene set enrichment analysis web server 2016 update. Nucleic Acids Res. *44*, W90–W97.

STAR★METHODS

KEY RESOURCES TABLE

REAGENT or RESOURCE	SOURCE	IDENTIFIER
Antibodies		
Human monoclonal anti-CD107a conjugated to PE (clone H4A3)	Biolegend	Cat#328608; RRID: AB_1186040
Human monoclonal anti-CD56 conjugated to APC-A750 (clone N901)	Beckman Coulter	Cat#B46024
Human monoclonal anti-CD56 conjugated to BV421 (clone NCAM16.2)	BD Biosciences	Cat#562751; RRID: AB_2732054
Human monoclonal anti-CD56 conjugated to APC-Fire750 (clone QA17A16)	Biolegend	Cat#392408; RRID: AB_2728404
Human monoclonal anti-IFNγ conjugated to PE (clone B27)	Biolegend	Cat#506507; RRID: AB_315440
Mouse IgG1, κ isotype control antibody conjugated to PE (clone MOPC-21)	Biolegend	Cat#981804; RRID: AB_3076354
Human monoclonal anti-TNFα conjugated to AF647 (clone Mab11)	Biolegend	Cat#502916; RRID: AB_493123
Mouse IgG1, κ isotype control antibody conjugated to AF647 (clone MOPC-21)	Biolegend	Cat#400130; RRID: AB_2800436
Human monoclonal anti-Perforin conjugated to PerCP-Cy5.5 (clone B-D48)	Biolegend	Cat#353314; RRID: AB_2571971
Mouse IgG1, κ isotype control antibody conjugated to PerCP-Cy5.5 (clone MOPC-21)	Biolegend	Cat#400150; RRID:AB_893664
Human monoclonal anti-Granzyme B conjugated to AF647 (clone GB11)	Biolegend	Cat#515406; RRID: AB_2566333
Human monoclonal anti-CD45 conjugated to KrO (clone J.33)	Beckman Coulter	Cat#A96416; RRID: AB_2888654
Human monoclonal anti-FLAG conjugated to FITC (clone REA216)	Miltenyi Biotec B.V.	Cat#130-127-901; RRID: AB_2905186
Human monoclonal IgG1 isotype control conjugated to FITC (clone REA293)	Miltenyi Biotec B.V.	Cat#130-113-437; RRID: AB_2733689
Rabbit monoclonal anti-G4S conjugated to AF488 (clone E7O2V)	Cell Signaling Technology	Cat#50515; RRID: AB_2941670
Rabbit monoclonal IgG isotype control conjugated to AF488	Cell Signaling Technology	Cat#4340; RRID: AB_561545
Human monoclonal anti-DNAM-1 conjugated to PE (clone DX11)	BD Biosciences	Cat#559789; RRID: AB_397330
Human monoclonal anti-CD3 conjugated to PerCP Cy5.5 (clone SK7)	Biolegend	Cat#344808; RRID: AB_10640736
Human monoclonal anti-CD14 conjugated to PerCP Cy5.5 (clone HCD14)	Biolegend	Cat#325622; RRID: AB_893250
Human monoclonal anti-CD15 conjugated to PerCP Cy5.5 (clone HI98)	Biolegend	Cat#301922; RRID: AB_2783153
Human monoclonal anti-CD19 conjugated to PerCP Cy5.5 (clone HIB19)	Biolegend	Cat#302230; RRID: AB_2073119
Human monoclonal anti-NKp30 conjugated to BV605 (clone P30-15)	BD Biosciences	Cat#563384; RRID: AB_2738170
Human monoclonal anti-NKp46 conjugated to BV785 (clone 9E2)	Biolegend	Cat#331946; RRID: AB_2810509
Human monoclonal anti-NKp44 conjugated to PE-Cy7 (clone P44-8)	Biolegend	Cat#325116; RRID: AB_2616754

(*Continued on next page*)

Continued

REAGENT or RESOURCE	SOURCE	IDENTIFIER
Human monoclonal anti-NKG2D conjugated to APC (clone 1D11)	Biolegend	Cat#320808; RRID: AB_492962
Human monoclonal anti-TRAIL conjugated to APC (clone RIK-2)	Biolegend	Cat#308210; RRID: AB_2564398
Human monoclonal anti-CD16 conjugated to BV421 (clone 3G8)	Biolegend	Cat#302038; RRID: AB_2561578
LIVE/DEAD™ Fixable Aqua Stain	Thermofisher	Cat#L34957
ViaKrome 808 Fixable Viability Dye	Beckman Coulter	Cat# C36628
Bacterial and virus strains		
Incucyte® Nuclight Red (NLR) Lentivirus	Essen Biosciences	Cat#4476
Biological samples		
Fresh umbilical cord blood	Anthony Nolan cord blood bank	N/A
Human AB serum	Akron Biotech	Cat#AR1048-0100
Chemicals, peptides, and recombinant proteins		
7-aminoactinomycin D	Sigma	Cat#A9400-1MG
Ficoll Paque Plus	GE Healthcare	Cat#GE17-1440-03
Pacific blue succinimidyl ester (PBSE)	Thermo Fisher Scientific	Cat#P-10163
Phorbol-12-myristate-13-acetate (PMA)	Merck Life Sciences	Cat#P1585-1MG
Ionomycin	Merck Life Sciences	Cat#I9657
Live/dead fixable aqua	Thermo Fisher Scientific	Cat#L34957
rhG-CSF	Miltenyi Biotec B.V.	Cat#130-093-860
rhGM-CSF	CellGenix	Cat#1012-050
rhIL-6	CellGenix	Cat#1004-050
rhIL-7	CellGenix	Cat#1010-050
rhSCF	CellGenix	Cat#1018-050
rhTPO	CellGenix	Cat#1017-050
rhFlt-3L	CellGenix	Cat#1015-050
rhIL-15	CellGenix	Cat#1013-050
rhIL-2	CellGenix	Cat#1020-050
CD9-HA2H9	AcroBiosystems	Cat#CD9-HA2H9-200tests
BX795	InvivoGen	Cat#tlrl-bx7
SsoAdvanced Universal SYBR Green Supermix	Bio-Rad	Cat#1725274
Critical commercial assays		
$CD34^+$ microbead kit	Miltenyi Biotech B.V.	Cat#130-046-702
Cytofix/Cytoperm™ Fixation/ Permeabilization Kit	BD Biosciences	Cat#554715
LV-MAX™ Transfection Reagent	Gibco	Cat#A35348
DNeasy Blood and Tissue Kits	Qiagen	Cat#69504
MycoAlert Mycoplasma Detection Kit	Lonza	Cat#LT07-318
Experimental models: Cell lines		
Daudi	ATCC	Cat#CCL-213
NALM-6	DSMZ	Cat#ACC 128
K562	ATCC	Cat#CCL-243
Raji	ATCC	Cat#CCL-86
Suspension HEK293-derived Viral Production Cells	Gibco	Cat#A35347
Adherent HEK293T	TaKaRa Bio	Cat#632180
NK-92	ATCC	Cat#CRL-2407

(*Continued on next page*)

Continued

REAGENT or RESOURCE	SOURCE	IDENTIFIER
Experimental models: Organisms/strains		
NOD-Prkdcem26Cd52Il2rgem26Cd22/ GptCrl NCG mice	Charles River Laboratories	N/A
Oligonucleotides		
Primer Psi forward: CGAACAGGGACTTGAAAGCG	This paper	N/A
Primer Psi reverse: AATACTGACGCTCTCGCACC	This paper	N/A
Primer RPP30 forward: CCAAATGTCCAGAACAGTGC	This paper	N/A
Primer RPP30 reverse: CTGCACACCATCGACAGACT	This paper	N/A
Recombinant DNA		
Plasmid: LV-GS-CMV-Luc-SV40-eGFP	This paper	N/A
Plasmid: pMDLg/pRRE	Addgene	Cat#12251
Plasmid: pRSV-Rev	Addgene	Cat#12253
Plasmid: pMD2.G	Addgene	Cat#12259
Plasmid: LV-GS-MNDU3-eGFP	This paper	N/A
Plasmid: LV-GS-CMV-eGFP	This paper	N/A
Plasmid: LV-GS-EF1α-eGFP	This paper	N/A
Plasmid: LV-GS-SV40-eGFP	This paper	N/A
Plasmid: LV-GS-PGK-eGFP	This paper	N/A
Plasmid: CAR1 LV-GS-MNDU3-CD19.CD8a. CD3ζ.(CD3ζ)-FLAG	This paper	N/A
Plasmid: CAR2 LV-GS-MNDU3-CD19.CD8a. CD28.(CD28.CD3ζ)-FLAG	This paper	N/A
Plasmid: CAR3 LV-GS-MNDU3-CD19.CD8a. CD137.(CD137.CD3ζ)-FLAG	This paper	N/A
Plasmid: CAR4 LV-GS-MNDU3-CD19.CD8a. CD28.(CD3ζ)-FLAG	This paper	N/A
Plasmid: CAR5 LV-GS-MNDU3-CD19. CD8a.CD28.(CD3ζ)	This paper	N/A
Plasmid: CAR6 LV-GS-MNDU3-CD19. CD8a.CD28.(CD3ζ^{mut})	This paper	N/A
Software and algorithms		
Graphpad Prism software 10.2	GraphPad Software	RRID: SCR_002798
Kaluza v2.1	Beckman Coulter	RRID: SCR_016182
BioRender	BioRender	BioRender.com; RRID:SCR_018361
BioNavigator 6.3	PamGene B.V.	N/A
CORAL	Phanstiel Lab	http://phanstiel-lab.med.unc.edu/CORAL/
Enrichr	maayanlab	https://maayanlab.cloud/Enrichr/
IncuCyte	Sartorius	RRID:SCR_019874
CFX Maestro 2.0	Bio-Rad	https://www.bio-rad.com/en-nl/product/cfx-maestro-software-for-cfx-real-time-pcr-instruments

(*Continued on next page*)

Continued

REAGENT or RESOURCE	SOURCE	IDENTIFIER
Other		
DMEM	Lonza/Westburg	Cat# LO BE12-604F/U1
RPMI 1640	Gibco	Cat#22-400-089
IMDM	Gibco	Cat#11504556
LV-Max Production Medium	Gibco	Cat#A3583401
FBS	Gibco	Cat#10500-064
TryplExpress	Thermo Fisher Scientific	Cat#10718463
Glycostem Basal Growth Medium	FertiPro	Cat#GBGM-500
CellGenix® GMP SCGM	CellGenix	Cat#20802-0500
CryoStor® 10	BioLifeSolutions	Cat#210102

EXPERIMENTAL MODEL AND STUDY PARTICIPANT

Ethics statement

Glycostem is working with cells from commercial tissue banks and blood products. This work is in general regulated by the Dutch law. Glycostem obtained cord blood from Anthony Nolan, Nottingham, UK. The ethical procedures regarding the donors are regulated and under the responsibility of the blood banks. All cord blood samples are obtained anonymously.

CELL LINES

The chronic myelogenous leukemia cell line K562, B cell Acute Lymphoblastic Leukemia cell line NALM-6, and the Burkitt Lymphoma cell lines Daudi and Raji, the NK-92 Malignant non-Hodgkin lymphoma cell line, suspension HEK293-derived viral production cells, adherent HEK293T were purchased from the relevant suppliers. All cell lines were banked at receipt and frozen stocks were generated from early-passage cells for future use. Samples from all banked cell lines were authenticated by short tandem repeat (STR) DNA profiling analysis according to the global standard ANSI/ATCC ASN-0002.1-2021 (2021) and resulted in an authentic STR profile of the reference database. All cultured cell lines were regularly checked for mycoplasma contamination by using MycoAlert Mycoplasma Detection Kit (Lonza). All cell lines were maintained in a humidified atmosphere containing 5% CO_2 at 37°C, except for suspension HEK293-derived Viral Production Cells, which were cultured at 8% CO_2. Fresh UCB units were purchased from Anthony Nolan cord blood bank.

IN VIVO ANIMAL STUDIES

All animal experiments were performed under the authorization of the French Ministry of Higher Education, Research, and Innovation (approval no. 38383 – 2022082413416895) and the Departmental Directorate for the Protection of Populations in Haute Savoie (approval no. A 7418 324), and in accordance with Association for Assessment and Accreditation of Laboratory Animal Care International (AAALAC International) accreditation (reference no. 001909). Female adult specific opportunist and pathogen free (SOPF) NOD-Prkdcem26Cd52Il2rgem26Cd22 (NCG) mice were obtained from Charles River, housed under SOPF conditions at TransCure bioServices.

METHOD DETAILS

Cell lines

K562 was cultured in Iscove's Modified Dulbecco's Medium (IMDM)(Gibco) containing 10% fetal bovine serum (FBS)(Gibco). Daudi, Raji and NALM-6 were maintained in Roswell Park Memorial Institute (RPMI) 1640 (Gibco) containing 10% FBS. The NK-92 Malignant non-Hodgkin lymphoma cell line was cultured in CellGro SCGM medium (Cellgenix) supplemented with 20% FBS and 1000 U/mL recombinant human interleukin 2 (rhIL-2) (Miltenyi Biotec B.V.). Suspension HEK293-derived Viral Production Cells (Gibco) were cultured in LV-Max Production Medium (Gibco) and adherent HEK293T cells (TaKaRa Bio) were cultured in Dulbecco's Modified Eagle's medium (DMEM) (Lonza) containing 10% FBS. For IncuCyte® assays, NALM-6, Raji and Daudi cell lines were transduced with IncuCyte Nuclight Red (NLR) Lentivirus (Essen Biosciences) to stably express the red fluorescent and nuclear-restricted protein mKate2. NLR positive cells were selected using 0.5μg/mL puromycin (Sigma-Aldrich) and banked for future use. NLR-cell lines were thawed and maintained for 1-6 weeks prior to use in the assays. CD19 target antigen expression was checked before use in the assays. For *in vivo* detection by bioluminescence, NALM-6 cells were modified to express luciferase (Luc) and enhanced green fluorescent protein (eGFP) (Luc^+/$eGFP^+$ NALM-6).

GS lentiviral plasmid backbone construction and CAR cassette design

To ensure clinical safety of the genetically engineered NK cells, we designed a lentiviral plasmid backbone (Glycostem, or GS) containing the necessary elements for plasmid propagation and transgene expression in a third-generation system, and the bacterial selection marker Kanamycin. Briefly, the integrating and regulatory elements portion, flanked by the 5'- and 3'-long terminal repeats (LTR) (truncated 5'-LTR and self-inactivating 3'-LTR from HIV-1), was constructed with the packaging element (Psi), the Rev Response processing Element (RRE), the central polypurine tract (cPPT) for recognition of DNA synthesis site, the transgene promoter, and the gene of interest (GOI) cassette.

Five different versions were designed, each carrying a different transgene promoter: the human cytomegalovirus (CMV) enhancer plus promoter, the synthetic MNDU3[23] containing the U3 region of a modified Moloney murine leukemia virus (MoMuLV) LTR plus the myeloproliferative sarcoma virus enhancer, the human phosphoglycerate kinase gene (PGK) promoter, the human elongation factor alpha 1 (EF1a) gene promoter, and the simian vacuolating virus 40 (SV40) promoters. The eGFP sequence was obtained from TaKaRa Bio.[24] Anti-CD19 CAR cassettes containing the CD8α signal peptide, the single-chain variable fragment (scFv) of the CD19-specific antibody clone FMC63 (with the heavy and light chains linked with a G4S linker (repeated 4 times), and with or without FLAG tag on the N-terminus of the scFv), CD8α hinge, CD3ζ or CD28 TMD, CD28 or 4-1BB and CD3ζ SD were codon optimized for expression efficiency. Signaling-defective CD3ζ SD was obtained by point mutation of tyrosine residues to phenylalanine on immunoreceptor tyrosine-based activation motives (ITAM) (3 on ITAM1, 2 on ITAMs 2 and 3). Plasmid and transgene DNAs were obtained from IDT or VectorBuilder; fragment insertion was performed by restriction and insertion cloning.

Lentiviral vector production and titer determination

For lentiviral vector production, a high-density culture of suspension HEK293-derived Viral Production Cells (1.2×10^8 cells per transfection in a final volume of 30 mL) was co-transfected with the lentiviral vectors, i.e., the pMDLg/pRRE plasmid (22.5 μg) containing the sequence for gag-pol, the pRSV-Rev plasmid (11.25 μg) containing the sequence for Rev, the pMD2.G plasmid (11.25 μg) containing the sequence for VSV-G envelope and the GS transfer plasmid (30 μg) containing the gene of interest, using LV-MAX™ Transfection Reagent (Gibco) at 37°C in an incubator with ≥80% relative humidity, 8% CO_2 and shaking at 125 rpm, according to the manufacturer's instructions. A 3:2 ratio of LV packaging to LV transfer plasmid was used according to Gibco's manufacturing instructions. Supernatant containing the secreted lentiviral particles was harvested 48 hours later and concentrated (100x) using Lenti-X Concentrator (Takara Bio Inc.). Lentiviral particles were resuspended in PBS and frozen at -80°C. To determine lentiviral titers, an aliquot of frozen lentiviral supernatants was used to transduce HEK293T cells with a serial dilution in the presence of 10μg/mL polybrene (Merck). The percentage of transduced cells was measured on flow cytometer Cytoflex LX (Beckman Coulter) and quantification of viral titers (infectious particles per mL) was calculated as follows: ((total number of cells/100) x percentage of transduced cells) x dilution of viral supernatant. To achieve efficient transduction, lentiviral titers were used at a minimum of 5×10^7 TU/mL and above.[37]

Lentiviral transduction of NK-92 cells

0.25×10^6 NK-92 cells per well were seeded in a 24-well plate (Corning) and transduced at multiplicity of infection (MOI) 20 with lentiviral supernatants in the presence of 8 μg/mL protamine sulfate and 6 μM BX795 (InvivoGen). Cells were incubated at 37°C, 5% CO_2 for 6 hours. At the end of incubation, transduction medium was replaced by fresh CellGro SCGM medium supplemented with 20% FBS and 10^3 U/mL rhIL-2. CAR transduction efficiency was measured 72 hours post transduction by measuring of FLAG-tag on live $CD56^+$ cells using flow cytometry and followed weekly until the cells were discarded 3 weeks post transduction.

Lentiviral transduction of UCB-derived primary $CD34^+$ cells for CAR-NK generation

$CD34^+$ HSCs were isolated from fresh umbilical cord blood (Anthony Nolan Cord Blood Bank) and were cryopreserved for future use or transduced to generate CAR-NK cells. $CD34^+$ HSCs (0.1×10^5 cells/ml) were seeded in a 24-well plate (Corning) and transduced early in the culture process (0-4 days) with or without lentiviral particles at MOI 0.5-20 to generate Mock control or CAR-NK cells. Cells were incubated at 37°C, 5% CO_2 for 24 hours at which point transduction medium was replaced by fresh culture medium. Cells were expanded and differentiated in Glycostem Basal Growth Medium (GBGM, FertiPro) supplemented with 10% human AB serum (Akron Biotech) and cytokines (all from CellGenix except for rhG-CSF)(at the following concentrations: 280 pg/mL rhG-CSF, 10 pg/mL rhGM-CSF, 50 pg/mL rhIL-6, 25 ng/mL rhIL-7, 25 ng/mL rhSCF, 25 ng/mL rhTPO, 25 ng/mL rhFlt-3L). Medium replacement was performed every 2-3 days during the whole culture period. After 9-10 days of culture, 20 ng/mL rhIL-15 (CellGenix) was added to replace rhTPO and after 14 days of culture, 1000 U/mL rhIL-2 (CellGenix) was supplemented to replace rhFlt-3L. Mock control or CAR-NK cells were cultured and, upon reaching >90% $CD56^+$ cells, were either cryopreserved as intermediate stocks or used fresh for further analytical assessments (Figure 1B). CAR expression on the transduced cells was confirmed as early as 1-week post-transduction and followed weekly by detection of FLAG-tag or G4S linker on live $CD45^+$ or $CD56^+$ cells by flow cytometry (Figure S1A). ΔMFI for $eGFP^+$ or CAR^+ cells was calculated as follows: ΔMFI = (the average of geometric mean of transgene expression of all cells from CAR transduction conditions) – ((the average of geometric mean of mock control conditions)). Cryopreserved Mock or CAR-NK cells were recovered and maintained for 3 or 7 days until viability, phenotypic or functional assessments were performed.

Cryopreservation of CAR-NK cells

CAR-NK cells were cryopreserved in CryoStor® 10 (BioLifeSolutions) cell freeze medium with the addition of 25% carrier solution containing saline 0.9% NaCl (Baxter) and 0.5% human serum albumin (Sanquin). The cells were frozen in cryovials with a controlled rate freezer and stored in the vapor phase of liquid nitrogen at below -150° C for long term storage.

Genomic DNA isolation and vector copy number determination by quantitative PCR

To determine VCN, genomic DNA (gDNA) was isolated from Mock and CAR-NK cells using the DNeasy Blood and Tissue Kits (Qiagen) according to the manufacturer's instructions and amplified using the SsoAdvanced Universal SYBR Green Supermix (Bio-Rad) on the CFX Connect Real-Time PCR Detection System (Bio-Rad). The Absolute Standard Curve Method[57] was used to determine the number of transgene integrations. Briefly, standard curves for lentiviral element Psi and reference gene RPP30 were generated by serial dilution of GS backbone and gDNA, respectively; linearity analysis was used to determine the number of copies in test samples. The following primers were used: Psi forward CGAACAGGGACTTGAAAGCG; Psi reverse AATACTGACGCTCTCGCACC; RPP30 forward CCAAATGTCCAGAACAGTGC; RPP30 reverse CTGCACACCATCGACAGACT. Each sample was amplified in technical triplicates and data was analyzed using the CFX Maestro software (Bio-Rad). A standard curve method was used to determine VCN values by converting Ct values to copy numbers using serial dilution of a plasmid of equimolar ratios of the RPP30 reference gene.

In vitro 24h flow cytometry-based cytotoxicity and 5h cytotoxicity/degranulation assay

The $CD19^+$ NALM-6 cells and $CD19^-$ K562 cells (used as a control) were washed and labeled with 5μM pacific blue succinimidyl ester (PBSE, Thermo Fisher Scientific) for 13 minutes in PBS followed by washing to remove excess dye. Target cell lines were then seeded in a tissue culture treated (TCT) flat-bottom 96-wells plate (Corning) and co-cultured with Mock control or CAR-NK cells (0.5×10^5 cells) at different Effector-to-Target ratios (E:T) for 24-hour (24h) flow-based cytotoxicity assay. At the end of incubation at 37°C, 5% CO_2, cells were transferred to a V-bottom 96-wells plate (Corning). For 5-hour (5h) flow cytometry-based cytotoxicity and degranulation assay, target cells were labeled with PBSE and seeded in a TCT V-bottom 96-wells plate (Corning). Effector only cells received 0.5 μg/mL PMA and 0.5μg/mL ionomycin (both from Merck Life Sciences) to induce maximum degranulation and were used as a positive control. After effector cell addition, anti-CD107a PE was added to each well to measure percentage of degranulating NK cells. For both assays, target cell lines or CAR-NK cells were cultured alone as controls, and all samples were seeded in technical triplicates. At the end of 5h or 24h incubations, plates were stained with 7-AAD (Sigma) (for dead cell discrimination), anti-CD56 APC-A750 (for NK cell detection). Samples were acquired on flow cytometer Cytoflex LX (Beckman Coulter) and data was analyzed using KaluzaV2.1 software (Beckman Coulter). Cytotoxicity percentage was calculated as follows: Cytotoxicity (%) = (1 - ((number of $7\text{-AAD}^-/\text{PBSE}^+$ target cells in co-culture)/(average number of $7\text{-AAD}^-/\text{PBSE}^+$ target cells alone)))*100. Degranulation was measured by gating on $CD56^+CD107a^+$ NK cells (Figure S5C). Antibodies used in the cytotoxicity assays are listed in the key resources table.

Assessment of intracellular expression of IFN-γ, TNF, perforin or Granzyme B

Measurement of the accumulating levels of IFN-γ and TNF was performed as previously described.[58] Shortly, cells were labelled with PBSE and co-cultured as described in *in vitro* 5h flow cytometry-based cytotoxicity/degranulation assay. For the measurement of perforin and Granzyme B, BD Golgistop™ was not added, to be able to quantify perforin and Granzyme B release after co-culture. After 5h incubation, cells were harvested and stained with anti-CD56 BV421 and live/dead fixable aqua marker (Thermo Fisher Scientific). Following cell fixation and permeabilization with the BD Fixation/Permeabilization Kit, cells were stained with isotype control or IFN-γ, TNF, perforin or Granzyme B antibodies (key resources table and Figure S5D). After washing twice with 1x perm/wash buffer, cells were resuspended in FACS Buffer for acquisition. All antibodies and kits were used at manufacturer recommended concentrations and instructions.

Phenotypic characterization of CAR-NK cells

Receptor expression on CAR-NK cells was measured by staining $0.5x10^5$ cells per sample at 4°C in the dark for 30 minutes, followed by washing. Cells were stained with anti-CD45 KrO, anti-CD56 APC-Fire750, viability dye Viakrome808 (Beckman Coulter) for dead cell exclusion and CAR expression was detected using either anti-FLAG (DYKDDDDK) FITC for CAR1, CAR2, CAR3 and CAR4 or anti-G4S linker AF488 (key resources table) for CAR5 and CAR6. CAR expression on transduced primary $CD34^+$ cells was first gated on FSC-A vs SSC-A followed by single cell gating via FSC-A vs FSC-H; then, $\text{ViaKrome808}^-/CD45^+$ living lymphocytes were distinguished and finally, $CD56^+CAR^+$ living NK cells were detected via CD56 vs CAR in weeks 2-5 post transduction (Figure S1A). $CD56^+CAR^+$ cell percentage was measured to determine CAR expression on NK cells at week 5 post transduction for functional assays or for further NK cell receptor expression analysis (Figure S4E). The panel of antibodies to detect NK cell receptor expression is listed in the key resources table. Samples were acquired on flow cytometer Cytoflex LX (Beckman Coulter) and analyzed with KaluzaV2.1 software (Beckman Coulter).

Protein kinase activity profiling using PamChip peptide microarrays

Kinome profiling was used to study protein kinase activity of CAR-NK cells and measured on a PamStation-12 with PamGene's Protein Tyrosine Kinase (PTK) PamChip and Serine Threonine kinase (STK) PamChip by Pamgene (PamGene International B.V., 's-Hertogenbosch, the Netherlands). Briefly, $1.2x10^6$ CAR-NK cells were treated with dH_2O or APC-Labeled Human CD19 (20-291) protein

(AcroBiosystems; Cat number CD9-HA2H9, UniProtKB:P15391-1, 1:20 dilution) for 5 or 20 minutes in 0.1mL of culture medium. The cells were washed once and pelleted for lysate preparation. Cells were lysed and protein quantification was performed according to PamGene protocol,[59] as previously described. Protein lysate was dispensed onto PamChip array dissolved in protein kinase buffer. Each PamChip array contains multiple peptide sequences that harbor phosphorylation sites corresponding to one or multiple kinases (196 peptides for PTK and 144 peptides for STK PamChip). A fluorescently labelled antibody (with or without a secondary detection antibody) was added to detect the phosphorylation signal of peptides phosphorylated by kinases present in the sample. Signals were recorded using a CCD camera and image-based analysis was used to integrate the obtained signals within the time course of the incubation of the kinase lysate on the chip into one single value for each peptide for each sample (exposure time scaling) using BioNavigator software 6.3 (PamGene). After low signal peptides were removed as quality control analysis, final peptide phosphorylation intensities were log2-transformed and median final score value was calculated as a combination of the intensity of the signal and of the specificity of the peptide mapping for each kinase on BioNavigator Analysis software tool. Top predicted kinases were visualized on a phylogenetic tree of human protein kinase families generated by CORAL.[60] Active kinases were selected based on a median final score > 1.3 and Log_2Fc >0.58. Downstream pathway analysis was performed using Enrichr.[61–63] Top 10 enriched pathways of the Reactome database are visualized.

Incucyte live cell cytotoxicity assays

NLR-cell lines were seeded at $0.4x10^4$ cells per well (NLR-NALM-6) or at $0.8x10^4$ cells/well (NLR-Daudi) in an ultra-low attachment U-bottom plate (Corning) and centrifuged for 10 minutes at 500xg. After 18-24 hours of incubation at 37°C and 5% CO_2, 3D aggregates were formed and co-cultured with Mock control or CAR-NK cells at an E:T of 1:3 for NLR-NALM-6 and at 1:1 for NLR-Daudi, unless specified otherwise. Live cell imaging of cytotoxicity was measured as the 'Total Red Object Integrated Intensity' (RCU x μm2/Image) every 1 hour for the indicated period at 4x magnification by the IncuCyte S3 live-cell analysis system (Essen Biosciences). Target cell fluorescence intensity data is plotted by normalizing to timepoint 0h plotted against the co-cultivation time in hours.

For the titration of CAR4 NK cells (Figures 6C–6F and 6I), cell suspensions for Mock and CAR4 NK cells of the same donor were prepared at the same cell concentration and CAR% was adjusted from 90% all the way down to 10% by decreasing the number of CAR4 NK cells and increasing the number of Mock cells in the mixture, while not exceeding a total of 3000 cells per condition. All conditions were performed in quadruplicates.

For 3D repetitive challenge assays, NLR-NALM-6 cells were seeded at $0.4x10^4$ cells per well and Mock control or CAR-NK cells were co-cultured at E:T of 1:1. New 3D aggregates were generated 18-24 hours prior to each new challenge. Every 5-6 days, effector cells were recovered from the co-cultures, resuspended in fresh medium before they were added onto new 3D aggregates. Fresh medium was supplemented 3-4 days after every effector addition. Target cell fluorescence intensity for 3D repetitive challenge assay analysis was calculated by first normalizing each measurement to its timepoint 0h and then, by normalizing to the average of targets only control. For 2D repetitive challenge assays, CAR-NK cells were co-cultured at E:T of 2:1 and 5:1; 5000 fresh NLR-Raji cells were added to the co-culture at each rechallenge. Target cell intensity for 2D represents the signal intensity of NLR-Raji cells measured in real time.

Tumor xenograft mouse model

To assess the efficacy of Mock control and CAR-NK cells *in vivo*, a survival study was performed by TransCure bioServices (TCS), in accordance with internal standard operating procedures. Briefly, $0.2x10^6$ human NALM-6 Luciferase$^+$ eGFP$^+$ (Luc$^+$/eGFP$^+$) cells were injected intravenously (i.v.) on Day -1 in immunocompromised adult NOD-Prkdc^{em26Cd52}Il2rg^{em26Cd22}/GptCrl NCG mice from Charles River Laboratories. On Days 0 and 7, mice from the respective treatment groups were treated with $1x10^7$ thawed and recovered cells. NK cells were maintained *in vivo* by intraperitoneal (i.p.) administration of 2500 units of rhIL-15 (Miltenyi Biotec B.V.) starting at Day 0 and every 2-3 days thereafter until Day 21 of the study. Intravital bioluminescence imaging was performed using a Vilber Newton 7.0 imaging system for *in vivo* monitoring of tumor growth in mice under anesthesia every 3-4 days starting from Day 6. Blood samples were acquired from the teil vein on Day 14 for flow cytometry-based analysis of peripheral blood circulating NK cells and NALM-6 tumor cells.

QUANTIFICATION AND STATISTICAL ANALYSIS

For preparation of graphs and statistical analysis, GraphPad Prism v.9.1 (GraphPad Software Inc.) was used. The type of statistical test used is indicated in the corresponding figure legend where n represents the number of NK-cell donors or animals used in the set-up. All data depicted is shown as mean ±SD. P-values lower than 0.05 were considered statistically significant.